STUDY ON HONEYCOMBS IN STRUCTURAL CONCRETE ELEMENTS

Kuruppu Appuhamillage Bandhuka Prashastha Kuruppu

208017B

Master of Philosophy

Department of Civil Engineering
Faculty of Engineering

University of Moratuwa
Sri Lanka

August 2024

STUDY ON HONEYCOMBS IN STRUCTURAL CONCRETE ELEMENTS

Kuruppu Appuhamillage Bandhuka Prashastha Kuruppu

208017B

Thesis submitted in partial fulfillment of the requirements for the degree
Master of Philosophy

Department of Civil Engineering
Faculty of Engineering

University of Moratuwa
Sri Lanka

August 2024

DECLARATION

I declare that this is my own work and this Thesis does not incorporate without acknowledgement any material previously submitted for a Degree or Diploma in any other University or Institute of higher learning and to the best of my knowledge and belief it does not contain any material previously published or written by another person except where the acknowledgement is made in the text. I retain the right to use this content in whole or part in future works (such as articles or books).

Signature: ***UOM Verified Signature*** Date: 22/08/2024

The supervisor should certify the Thesis with the following declaration.

The above candidate has carried out research for the Master of Philosophy Thesis under my supervision. I confirm that the declaration made above by the student is true and correct.

Name of Supervisor: Dr. K. Baskaran

Signature of the Supervisor: ***UOM Verified Signature*** Date: 22|08|2024

DEDICATION

To Dr. K. Baskaran, whose inspiration ignited my passion for research from undergraduate to postgraduate levels and for emphasizing the vital importance of conducting research directly targeting the construction industry. This thesis is dedicated to you with immense gratitude for your guidance and unwavering support.

ACKNOWLEDGEMENT

First and foremost, I am deeply grateful to Dr. Udaya Chinthaka Jayathilaka from the Mathematics Department at the University of Moratuwa for his invaluable guidance and expertise in the mathematical aspects of this research. His mentorship and insightful input have been integral to the success of this thesis.

I would also like to acknowledge the outstanding support provided by the laboratory staff of the Department of Civil Engineering at the University of Moratuwa. Their assistance in conducting experiments and providing resources has been indispensable in ensuring the quality and accuracy of the research conducted.

Additionally, I extend my thanks to the Lanka Steel Corporation for their generous provision of reinforcement materials for the experiments. Their collaboration has significantly enhanced the practical aspects of this research.

ABSTRACT

Concrete structures are subjected to various types of surface defects such as honeycombs, surface voids, form streaking, etc. Proper understanding of the root causes of each type of defect is significant in preventing recurrence as well as applying remedies. An extensive field survey was conducted in connection with the construction sector of Sri Lanka to gather information on the current practices. It was found that the construction industry needs more awareness on correct practices. This study attempts to fill the gap between current field practices and standard practices. Poor workmanship in consolidation of fresh concrete leads to most of the defects, but this study shows how the understanding of technical background of each activity and the proper planning at initial stages contribute to effortless improvements in workmanship. Contradictions between codes of practices for design of reinforced concrete and codes of practices for consolidation of concrete were also discussed under this study. In order to identify the impact from reinforcement on UPV tests on concrete, a series of UPV tests (conventional approach) were done, and the drawbacks of that approach are highlighted under this study. As a modern approach, vibration pattern analysis of structural elements has emerged as a valuable technique for various purposes within the field of structural engineering. The analysis of vibrational patterns can be employed for different objectives, including damage detection, modal parameter identification, health monitoring, and structural integrity assessment. The presence of non-homogeneity in structural elements poses unique challenges in terms of analysing their behaviour, predicting their response to loads, and detecting damage or deterioration accurately. The straight-forward mathematical models based on first principles are for homogeneous elements having uniformly distributed mass and uniform distribution of stiffness. This study has developed a novel mathematical approach based on first principles for mode shapes of beams having deviated regions of mass and stiffness. This insight can help to identify key factors influencing the mode shapes and their variations. Furthermore, this study has done an extensive study on mode shape curvature analysis for identification of hidden honeycombs in concrete structures. The findings of this analysis fill research gaps in the study area. Moreover, the novelty of that approach is its extension to the analysis of portal frames. Consequently, a combination of conventional non-destructive tests and mode shape curvature analysis will provide a robust approach for hidden defect detection and assessment in structural concrete elements.

Keywords: Honeycombs, Mode shape curvature, Vibration, Mathematical Approach, UPV, Concrete, Compaction, First Principles

TABLE OF CONTENTS

LIST OF FIGURES

LIST OF TABLES

LIST OF APPENDICES

CHAPTER 1

INTRODUCTION

1.1 Background

Honeybees build honeycombs as a series of hexagonal cells in order to store their honey and larvae. Each cell in the honeycomb is six-sided and connected to each other. Figure 1.1 shows the Honey bee's bee hive with a hexagonal pattern.

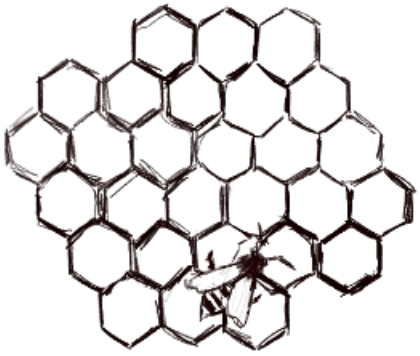

Fig. 1.1: Bee hive with hexagonal pattern

In the construction industry, the term "Honeycomb" is used in two ways such as to describe structural core material that is lightweight, yet strong and stiff (Honeycomb structures) and to describe defects in concrete structures that occur when voids or pockets are left in the concrete. This study focuses on the construction defects termed "Honeycombs" in the construction industry.

Honeycombs in construction defects refer to a type of defect in concrete that occurs when cavities are left in either the surface or inside of concrete mass after pouring and compaction of concrete. These voids can create a pattern that resembles the cells of a honeycomb, hence the name. One of the common and critical defects in concrete structures is honeycomb damage. In the construction industry, there are numerous examples of instances where these honeycombs are not properly identified during the construction period, which can be costly to repair in a later part. Failure to identify these defects can lead to construction collapse and loss of life and property. Hence, at present, the construction industry requires excessive awareness of these honeycombs and ways of avoiding/overcoming them. Figure 1.2 shows a surface defect of a concrete retaining wall. In order to minimize such construction defects, proper investigation of the root cause of honeycombs is crucial. There are various factors causing these construction defects which have been discussed in this study.

The identification of construction defects like Honeycombs is linked with the de-

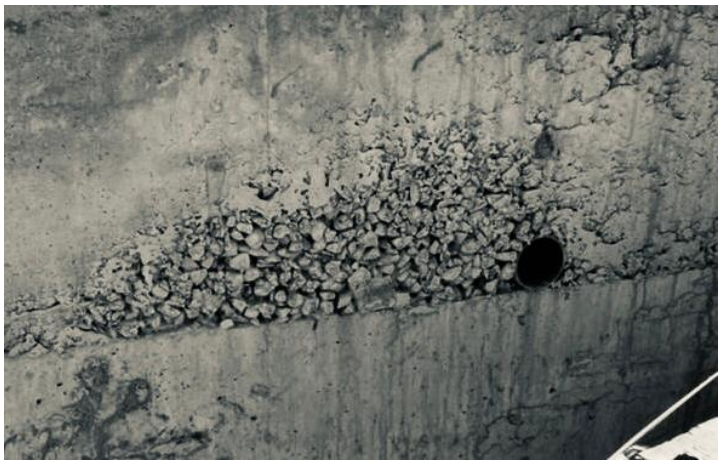

Fig. 1.2: A honeycomb in the surface of a retaining wall

velopment of concrete as a building material and the development of construction practices. During the early years of construction, there was limited knowledge and understanding of the processes and the materials used in concrete, so did the understanding of the formation of construction defects. As knowledge of concrete technology was developed, the world moved towards major constructions using concrete, and the identification of construction defects like honeycombing and remedial actions was also significant. In the mid-20th century, research works have been carried out to study the effects of honeycombing on structural integrity and related risks and consequences of construction defects. Talbot [2] and Potter [3] have done studies on concrete and defects like honeycombing in early-20th century. Hebard [4] has defined honeycombs as voids in concrete that are caused by the failure of the concrete to bond to the formwork through his publication in 1924. More information on the early studies has been elaborated later in this report.

1.2 Problem Statement and Research Gap

Identification and Prevention of Honeycombs in structural concrete elements has been a hot topic with the development of concrete technology and construction practices. Many studies have been carried out to identify the root causes for such construction defects. Furthermore, guidelines/standards have been established by various institutions in order to minimize the occurrences of honeycombs in structural concrete elements.

If we consider the local construction industry, through an extensive field survey under this study, it was found that most of the contractors are not following standard practices in concrete works, and are lack of knowledge in technical background of the formation of construction defects. This study has provided a set of guidelines for local contractors and has attempted to fill that gap in the local construction industry.

The lack of raw materials for construction activities is a challenge that the world

is facing nowadays. In order to face this, there's a vast development in design optimization and ways of minimizing the demand for raw materials. Therefore, the identification and prevention of construction defects like honeycombs have become critical. There are some occasions where the honeycomb is not visible from the outside. The conventional approach in the identification of honeycombs is visual inspection. Therefore, most of the time, hidden honeycombs are hidden until a failure. However, there are some conventional, hidden defect detection methodologies in practice such as the Ultrasonic Pulse Velocity (UPV) test, Rebound hammer test, etc. This study shows the drawbacks of these conventional approaches.

There are fewer studies on hidden honeycomb detection methods. Pandey et al. [5] have shown a damage detection approach from changes in curvature mode shapes in 1991 and thereafter, several studies have been carried out on that, and as at present, there's a requirement of a modern hidden-damage detection method for concrete structures. Mode shape curvature analysis is a far better approach to fulfilling that requirement. This study contributed to developing that hypothesis with a novel mathematical approach focusing on the identification of the location and the severity of such defects. Apart from that, this study has done in depth analysis of the formation of honeycombs which helps to understand the governing factors so that remedial actions can be taken on a proper basis.

1.3 Objectives

Objectives of the study:

i. A step forward in the modern approach of hidden honeycomb detection - mode shape curvature analysis.

ii. Better understanding of the formation of honeycombs in structural concrete elements.

iii. Examination and evaluation of the drawbacks of conventional hidden honeycomb detection methods.

iv. Publication of a set of guidelines to avoid and mitigate the occurrences of honeycombs in structural concrete elements.

Overall, this study will aim to improve the theoretical understanding of honeycombs in concrete structures, recommendations for better practices in the local context, and to contribute in developing a modern approach for hidden honeycomb detection, based on mode shape curvature analysis by introducing a novel mathematical model.

1.4 Scope and Limitations

As elaborated in the previous section, this study has introduced a novel mathematical approach in identification of hidden honeycomb defects based on mode shape curvature analysis. The validation of the approach was done by incorporating finite element models. This study has not considered the validation through physical models as it requires advanced sensors and technology, which shall be done as the next step of this study.

Moreover, the extensive field survey on honeycomb defects was done in the local construction industry as the reporting of the current practices, level of understanding, and remedial actions in the local context are objectives of this study. Therefore, the recommended guidelines are more related to the local construction industry.

1.5 Significance and Contribution

The world is moving towards advancements in concrete technology and construction practices focusing on design optimizations and lesser use of raw materials. Parallel to that, the durability of structures has become a prime concern. Therefore, a better understanding of formation of construction defects, identification of hidden defects in concrete structures has become critical. There's a higher requirement for the development of damage detection parallel to the development of concrete technology.

This study contributed in stepping forward in hidden honeycomb detection in concrete structures based on mode shape curvature analysis. A novel mathematical model has been developed and used for this, which shows the location and severity of hidden defects in structural concrete elements.

Further, this study has developed a hypothesis for the formation of honeycombs in concrete structures based on several observations. This hypothesis can be effectively used in taking remedial actions for occurrences of honeycombs.

As per the extensive field survey done in the construction industry, it was observed that the contractors lack of technical knowledge behind their activities and are not following standard practices. This study contributed in setting a set of guidelines for local contractors to mitigate the chances of occurring honeycombs by addressing key points in the design and planning stage as well as in the operation stage.

1.6 Outline of the Thesis

- Chapter 1 gives an introduction and the background of the study, highlighting the research gap, objectives, scope, limitations, and significance.
- Chapter 2 elaborates on the literature review and the research gaps addressed in this study.

- Chapter 3 provides an experimental and theoretical approach to understanding the formation of honeycombs.
- Chapter 4 details the extensive field survey conducted, analyzes the findings of the field survey, and provides recommendations.
- Chapter 5 discusses the impact of reinforcement on UPV tests through an experimental approach.
- Chapter 6 presents a novel mathematical model for the derivation of the motion equation for non-homogeneous elements, relating to mode shape curvature analysis in damage detection.
- Chapter 7 offers a detailed explanation and analysis of hidden honeycomb detection based on mode shape curvature analysis, representing a step forward in studies of mode shape curvature analysis for hidden damage detection in structural concrete elements.
- Chapter 8 provides the conclusion of the study, elaborating on the key findings, and overall recommendations, and discussing how the novelty of this study contributes to further developments in this area.

CHAPTER 2

LITERATURE REVIEW

2.1 Pioneering Studies

A comprehensive study on concrete technology is imperative for investigating construction defects such as honeycombs. The use of concrete dates back to ancient times. Ancient civilizations such as the Egyptians, Greeks, and Romans all used a form of concrete in their building projects.

John Smeaton [6], who lived from 1724 to 1792, is known for his work on the Eddystone Lighthouse off the coast of Cornwall, England. He used hydraulic lime, which is a type of concrete, in the construction of the lighthouse in the mid-1700s. However, it is important to note that hydraulic lime is not the same as the modern Portland cement concrete that is widely used today.

Joseph Aspdin [7], who patented a method of making Portland cement in 1824, is generally credited with inventing modern concrete. His invention of Portland cement was a key development in the history of concrete, as it enabled the production of a durable, strong, and versatile building material that could be used for a wide range of construction projects.

Proper mixing of fresh concrete and construction defects are co-related to eachother. There are many studies on explaining what really happens to fresh concrete when vibrating, yet understanding of the interaction between vibration and fresh concrete is open for study. Walz [8] has shown that there's a reduction of friction between ingredients in the concrete mix as a result of acceleration produced during vibration. In his research, Kolek [9] identified two distinct stages in the process of concrete consolidation, namely slumping and entrapped air removal. Meanwhile, L'Hermite et al. [10] investigated the consolidation mechanism under vibration and observed that vibration induces particle motion and eliminates internal friction within the mix. Their study also highlighted the differences in concrete behaviour between static and vibrated conditions. According to them, concrete mix tends to act as a fluid during vibration. These findings have been crucial for developing standard practices for concrete works in order to mitigate construction defects like honeycombs.

2.2 Consolidation of fresh concrete

2.2.1 Constitutes of fresh concrete

The concrete mix consists of three basic components such as water, aggregate, and cement. As a result of mixing cement with water, the cement paste is composed and it

coats fine aggregates and coarse aggregates, further, through the hydration process, the cement paste gets hardened and acts as a binding agent for aggregates. The outcome of the entire process produces a composite solid material known as concrete.

To use concrete as a material for structural elements in a structure, it has to fulfil some other facts as well. The material has to be up to expected standards in strength wise, durability, workability, etc.

For a given concrete mix design, certain measures are expected at the stage of pouring concrete in order to ensure the designed quality of concrete at the post-pour stages. Expelling entrapped air from freshly placed concrete and maintaining the required density of concrete by packing its aggregates are important in this regard. Figure 2.1 is from a publication on Petrographic Methods of Examining Hardened Concrete by the U.S. Department of Transportation [1].

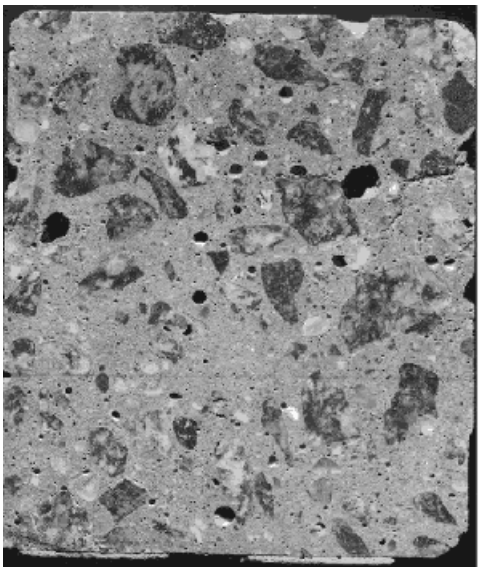

Fig. 2.1: Cross section of hardened concrete [1]

It shows a cross-section of hardened concrete. There, aggregates, cement paste, and bug holes are visible. Homogeneous mixing of these components and the expelling of entrapped air in concrete are important to assure the quality of the mix. Proper compaction of concrete does a major role in this regard.

When concrete is poured on any mold of a structural element, initially, the mix is not homogeneous. Air is entrapped in the mix which needs to be expelled. To overcome this condition, the mix needs to be vibrated sufficiently; known as the concrete compaction.

2.2.2 What happens when vibrating fresh concrete?

There are many studies on explaining what really happens to fresh concrete when vibrating, yet understanding of the interaction between vibration and fresh concrete is

open for study.

Freshly placed concrete often contains trapped air, leading to a honeycombed structure. If the concrete hardens in this state, it will become uneven, weak, porous, and have a poor bond with the reinforcement, as well as an unattractive appearance. To achieve the desired qualities of concrete, the mixture must be properly compacted.

Compaction, or consolidation, involves rearranging the solid particles in freshly mixed concrete or mortar to reduce air pockets. This is typically done using methods like vibration, rodding, tamping, or similar techniques. The same process can be applied to other cementitious mixtures, soils, or aggregates.

In 1963, in a conference held in Budapest, Hungary, several explanations on the subject were uncovered. Kolek [9] showed that the process of consolidation occurs in two stages; they are the slumping of concrete and the removal of entrapped air. Kirkham [11] showed the force applied to the concrete, amplitude of vibration, and the number of vibrations transmitted to the concrete are the most important factors affecting the degree of consolidation.

In 1976, Taylor [12] showed acceleration and amplitude as the most important parameters of internal vibrators. He had used Gamma-ray scanning to determine the density of concrete in his laboratory tests related to his study. In 1977, Alexander [13] commented on the mechanics of motion of fresh concrete. He showed that, during vibration, stiffness, and damping practically disappear and only mass was involved.

L'Hermite and Tournon [10] have done a study on the mechanism of consolidation under vibration and shown, that vibration sets particles in the mix to motion and eliminates internal friction of them. They have shown the differences between concrete at rest and during vibration. During vibration concrete undergoes two stages such as rapid subsidence of the uncompacted mixture (stage 1) and the removal of entrapped air (stage 2). Furthermore, they have shown that the internal friction during vibration is reduced to about 5% of the value at rest.

After this transformation, the vibratory motion was controlled by the mass forces with little or no effect from stiffness or damping, which tells that the concrete during vibration behaves like a fluid. Therefore, over-vibration leads to more and more subsidence of materials and ends in segregation.

ACI committee 309 sponsored an international symposium on concrete consolidation in San Francisco, 1986. Characteristics of fresh concrete during vibration were deeply discussed there. Iida and Horigome [14] found that dividing the mixing water into two parts and adding them to the no-slump lean concrete mixture at different stages enhances its compaction properties.

When the mortar does not fill the space between the coarse aggregate particles, honeycomb occurs. This indicates that consolidation has not been completed in these locations. However, although the concrete is free of honeycombs, still there can be air voids as complete removal of air voids is not that feasible. The amount of entrapped air

in the concrete mix mainly depends on the level of vibration, concrete mix constituents and the placement of concrete. The surface air-voids due to these are commonly called bug-holes. Keeping the vibrator closer to the form and progressing with layer thicknesses of 150mm will considerably reduce these surface air-voids.

The above studies help to understand the physical behaviour of ingredients of fresh concrete. These studies, models, and results are very significant in understanding the formation of honeycombs.

2.3 Main causes for honeycomb damages and standard practices

2.3.1 Main causes for honeycomb damage and preventive actions

Galappaththi et al. [15] have listed the main causes for structural defects and the remedies practised in the local construction sector. They have shown that the lack of adherence to quality assurance and quality control guidelines and relevant standard practices as a critical drawback in the Sri Lankan construction industry. They have identified that, poor QA/QC practices, detailing errors, poor coordination, poor workmanship, and unfavourable working conditions as the main factors for defects. Furthermore, the importance of contractors and workers following QA/QC practices, construction standards, and specifications to ensure fewer construction defects has been highlighted throughout their study.

Savitha [16] has highlighted the significance of the quality assurance of construction materials in order to minimize construction defects and to ensure the durability of products. Furthermore, Jamaluddin et al. [17] have shown the importance of taking action to minimize the possible failures of structures by conducting proper structural health monitoring of structures. They have identified the root cause for a failure of effluent tank concrete walls as occurrences of honeycombs due to improper consolidation of concrete or due to the use of stiff concrete.

2.3.2 Standard practices

The use of immersion vibrators for consolidating concrete is a critical process in construction, and adherence to standard practices is crucial to ensure the quality and durability of the resulting structures. One valuable resource in this regard is the Indian Standard, "Code of Practice for Use of Immersion Vibrators for Consolidating Concrete" [7]. This standard provides comprehensive guidelines and knowledge on the proper utilization of immersion vibrators, offering insights into standard ways of using these vibrators for effective concrete consolidation and it is more related to construction activities in Sri Lanka.

In addition to the Indian Standard, the American Concrete Institution (ACI) has published several reports that contribute to the understanding of concrete consolida-

tion, the behaviour of fresh concrete during vibration, and the identification and control of visual surface defects. One such report is the ACI Committee 309's publication, which offers extensive knowledge and guidance on the consolidation of concrete [8]. Furthermore, ACI Committee 309's reports [9] and [10] delve into the behaviour of fresh concrete during vibration and provide valuable insights on the identification and control of visual surface defects.

To ensure overall quality control and assurance in concrete construction, it is essential to consider relevant standards and best practices beyond consolidation techniques. ASTM C31/C31M-21, the "Standard Practice for Making and Curing Concrete Test Specimens in the Field" [18] provides guidelines for the proper creation and curing of concrete test specimens, aiding in quality assurance during the construction process. Neville's comprehensive reference, "Properties of Concrete" [19], and Mehta and Monteiro's book, "Concrete: Microstructure, Properties, and Materials" [20], offer in-depth insights into the properties and behaviour of concrete, including consolidation techniques and the occurrence of surface defects.

2.4 Detection of honeycombs in structural concrete elements

Whenever a honeycombing takes place on the surface of a concrete element, it can be easily observed (usually, when removing shuttering) by the execution team or QA/QC team. Thereafter necessary actions can be taken, but what if the honeycombing takes place inside the concrete mass? Then it can't be easily identified, sometimes it might be hidden until signs of a failure are exposed. However, if there's any doubtful situation, non-destructive tests (NDT) are carried out for further examination.

2.4.1 Conventional approaches

Commonly practised non-destructive tests are rebound hammer tests and ultrasonic pulse velocity (UPV) tests. However, it's difficult to test the entire element by these methods, only a selected location can be examined [21]. Therefore, for civil structures, a global non-destructive examination (NDE) technique utilizing the vibration characteristics of a structure is effective in assessing the condition of the overall structure [3]. But this does not mean that NDE techniques can't be utilized for single elements. Localized NDE techniques can be utilized upon identification of a damage location, to determine the specific nature of the damage in an element of a structure [1].

Rytter [22] has introduced a procedure for structural health monitoring by defining four levels as below;

Level I: Identify that damage has occurred.

Level II: Identify that damage has occurred and determine the location of damage.

Level III: Identify that damage has occurred, locate the damage, and estimate its severity.

Level IV: Identify that damage has occurred, locate the damage, estimate its severity, and evaluate the impact of damage on the structure or estimate the remaining useful life of the structure.

2.4.2 Modern approaches

The application of vibration characteristics is a commonly used method in nondestructive examination (NDE) on a global scale. It typically encompasses the following two aspects [23]:

1. Performing dynamic tests to gather modal parameters such as natural frequencies, mode shapes, and damping properties, or other characteristics like time histories and frequency response functions.

2. Employing a damage detection algorithm to ascertain the presence of damage within the structure, determine its location, and assess its severity.

Let's consider the above two features as two phases of non-destructive examination. The first phase is associated with dynamic testing of the structure which requires a source of excitation to vibrate the structure, the use of sensors, and experimental modal analysis procedures to extract modal parameters such as frequencies and mode shapes. The second phase is developing a damage detection algorithm referring to observations in the first phase.

In the field of structural dynamics, there are two primary types of dynamic tests conducted on structures. The first method is known as the input-output method, which entails applying a predetermined input, such as an impulse load or a known forcing function, to the structure. Following the application of this input, the resulting free vibration response of the structure is measured and analyzed [24]. This approach allows researchers to understand how the structure reacts and behaves under controlled external stimuli. Conversely, the second method, referred to as the output-only method, involves measuring the response of the structure under its normal operating conditions, without any predetermined inputs. This method relies on ambient excitation or naturally occurring forces acting on the structure during its regular usage [24], [25]. By capturing and analyzing the structural response in its natural environment, researchers gain insights into the dynamic behaviour of the structure under realistic conditions. Both of these dynamic testing methods contribute to the comprehensive evaluation and understanding of structural performance. This can be utilized for damage detection as well.

Another modern approach of damage detection is Computational intelligence methods such as neural networks and genetic algorithms are attractive processes in the area of structural damage detection because of their effectiveness and robustness in coping with uncertainty, and insufficient information [26]. In identifying, locating, and estimating the severity of damages in concrete structures, machine learning techniques take more attention of researchers. However high input information requirements and the development of powerful algorithms are challenges in demonstrating robustness with field-measured data [23].

Overall, this study will focus on developing a vibration-based, defect detection method.

2.4.3 Vibration-based damage detection

In 1991, Pandey et al. [5] proposed a novel approach to damage detection of concrete structures with the use of mode shape curvature analysis. Instead of analyzing the mode shape of structural elements, they have proposed to analyze the changes in the mode shape curvature which is a more sensitive parameter in the detection of changes. The improvements of this approach are still in progress by the researchers.

The basis of this vibration-based damage detection is the change in resonant frequency due to changes in its structural properties (i.e. damages under this context). But change in frequencies or mode shapes alone does not give accurate results on damage detection because several damages might give a frequency closer to the resonant frequency [24].

Therefore developing a powerful damage detection algorithm that is sensitive to small changes is an open area for researchers from the past few decades. There are many approaches for frequency-based damage detection; Hassiotis [27] formulated an optimization algorithm on the basis that damage resulted in localized changes in the stiffness matrix, where the stiffness matrix was resolved through natural frequency measurements and the classical eigenvalue problem was used to find the eigenvalue sensitivities to the stiffness matrix.

Sometimes, measuring mode shapes is a difficult task as a large number of measurements might be required to observe accurately characterized mode shapes [28]. Law et al. [29] proposed the expansion of measured modal data to match a finite element model; the modal strain energy of each element was normalized with its potential energy to locate a damage domain; the measured modal frequency changes were used to estimate damage severity using a sensitivity-based method.

Dawri and Vesmawla [30] have demonstrated honeycomb damage detection with the help of modal curvature and modal flexibility methods. The pre and post-damage eigenvectors were the basis for their damage detection. Mode shape curvature for the beam in the undamaged and damaged condition have been estimated numerically from

the displacement mode shapes under their study. The special thing here was that they had used a finite-element model simulating honeycombs in pre-defined locations of reinforced concrete beam model. Finite element model of an intact reinforced concrete beam had been developed using ANSYS. The honeycomb had been simulated by reducing the stiffness of the designated damaged elements. Then the absolute differences between the curvature mode shapes of the intact and the damaged beam had been plotted. The maximum difference for each curvature mode shape occurred in the damaged region. The difference in the curvature mode shapes had been localized near the damaged zone. In addition, they have shown that the higher modes were more sensitive to the damage.

Another study on the determination of damage location in RC beams using mode shape derivatives was done by Ismail et al [31]. They used a shaker and an accelerometer to record the response mode shape from the damaged reinforced concrete beam model. When compared with undamaged mode shapes, the mode shape differences were higher near damaged locations.

2.5 Research Gap and summary of Literature Review

As elaborated in this chapter itself and from the findings under field survey, rebound hammer test and ultrasonic pulse velocity (UPV) tests are the common practices for non-destructive examination of honeycombs and other defects. However, there are certain drawbacks in these approaches. Mode shape curvature analysis in identification of hidden defective regions in a structural element is still not well established. There are several studies on different approaches in mathematically modelling the mode shapes for non-homogeneous elements. However, that area is still open for study. This study attempts to fill that research gap by introducing a novel mathematical model for mode shape analysis of non-homogeneous elements.

Apart from that, another area that needs explanations is that, how the smooth thin cement paste layer is formed in mold surface when vibrating and what are the governing factors behind the formation of that layer. This study provides a hypothesis explaining this phenomenon. This follows several experimental observations as well.

Moreover, local construction practices often reveal a significant gap in understanding the underlying causes of certain observed defects. This study addresses this issue by offering guidelines to effectively reduce the occurrence of honeycombing in concrete. By identifying the key factors contributing to these defects, the study aims to enhance the quality and durability of concrete structures. Additionally, the proposed guidelines are designed to align with current industry standards, ensuring practical applicability and improving overall construction outcomes.

Knowledge of concrete technology is crucial for investigating honeycomb defects. The invention of Portland cement was a pivotal development in the history of concrete

technology. Today, numerous studies focus on the further advancement of concrete technology, as the world increasingly moves towards the construction of mega structures using concrete. Consequently, the development of methods for identifying and preventing construction defects has become a critical concern in the construction industry.

There have been many pioneering studies aimed at understanding the behaviour of fresh concrete during consolidation. The "Symposium on Vibration Compaction Techniques," held in Budapest, Hungary, in 1963, was a landmark event that provided in-depth explanations related to the compaction of concrete. The conclusions and recommendations from this symposium have had a significant impact on the current practices of vibration compaction. Subsequently, institutions such as the American Concrete Institute (ACI) have published reports and standards related to concrete compaction, the identification of construction defects, and remedial actions.

Traditionally, the construction industry has relied on conventional non-destructive damage detection methods, such as rebound hammer tests and ultrasonic pulse velocity (UPV) tests. However, field studies have highlighted certain limitations in these conventional approaches. As a result, the industry is increasingly adopting modern damage detection techniques based on analyzing vibrating patterns of concrete structures. These advanced methods are in high demand due to their accuracy and sensitivity, as the durability of concrete structures remains a primary objective in the advancement of concrete technology.

CHAPTER 3

UNDERSTANDING THE FORMATION OF HONEYCOMBS

3.1 Background and problem statement

A proper understanding of the formation of honeycombs is crucial for setting up damage detection methodologies. Mostly, the honeycombs encountered at construction sites can be visually inspected.

What makes it visible? It's clear that the smooth, thin cement paste layer is no longer on the surface of the concrete element whenever there is a honeycomb. Instead, the aggregates in the core are visible with air voids. Therefore, the unavailability of that smooth, thin layer of cement paste makes the surface honeycombs visible to the outside. Therefore, the formation of that layer of cement paste needs to be studied for a better understanding of the formation of honeycombs. As per the literature survey done, there's no proper explanation for the formation of this smooth layer of cement paste around the surface of the concrete element. Through this study, a hypothesis was developed to explain this scenario. The development of the hypothesis was based on the experimental results.

3.2 Experimental approach

As discussed in the literature review, Kolek [9] has shown the process of consolidation undergoes two stages such as the slumping of concrete and the removal of entrapped air. Here, we can observe the formation of a smooth thin cement paste layer in the inner face of the mold. An experiment was carried out to observe this. A mold was prepared having a transparent glass face on one side.

See Figure 3.1. The mold was filled with fresh concrete and vibrated. Gradually, it created a smooth, thin cement paste layer on the surface. This smooth, thin cement paste layer is the key visual observation during the detection of honeycombs from outside. If the consolidation process is not undergone properly, it will not create this layer properly. Hence, the honeycombing will be exposed.

Fig. 3.1: Formation of smooth, thin cement paste layer on the surface

Understanding the mechanism for creating this smooth, thin cement paste layer is important. As L'Hermite and Tournon [10] explained, the concrete mix tends to act as a fluid during vibration. As entrapped air releases from mid of the mix to the surfaces, the cement pastes and the slurry follows the air-entrapping path and meets the surface. We know that the coarse aggregates touching the mold surface are already coated with cement paste, therefore the cement paste and slurry coming through the mix to the surface makes a smooth layer of cement paste.

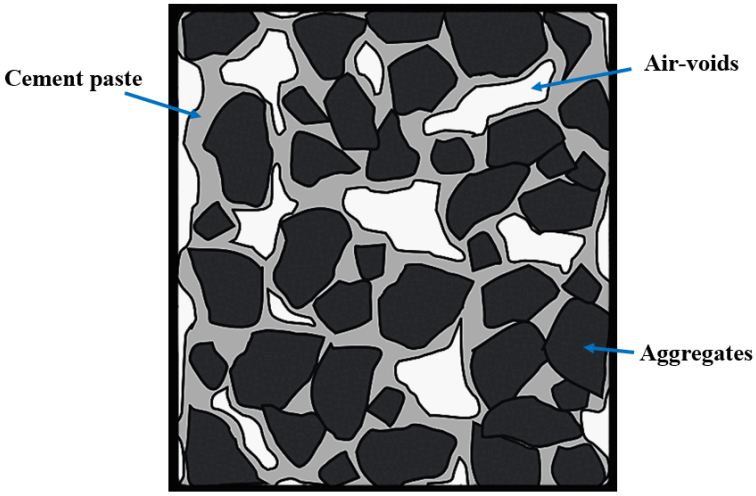

Fig. 3.2: Core arrangement of fresh concrete prior to vibration

Figure 3.2 shows the core arrangement of fresh concrete prior to vibration. Figure 3.3 shows how the cement paste and slurry follow the air-entrapping path during

vibration.

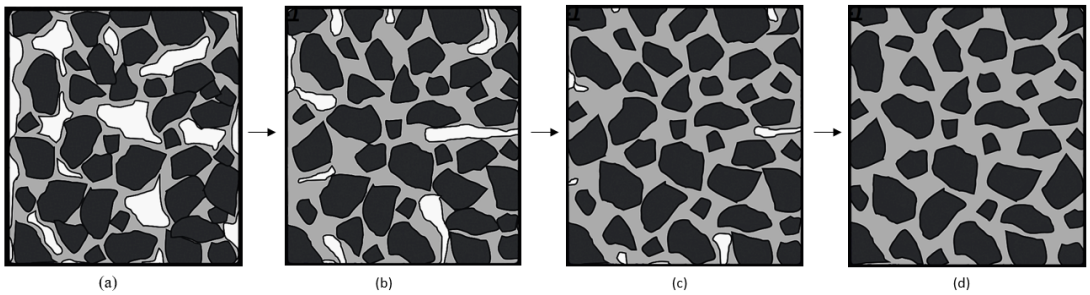

Fig. 3.3: Cement paste and slurry following the air-entrapping path during vibration

3.2.1 Hypothesis for development of smooth, thin cement paste layer on the surface

Figure 3.4 shows changes to the surface when undergoing vibration.

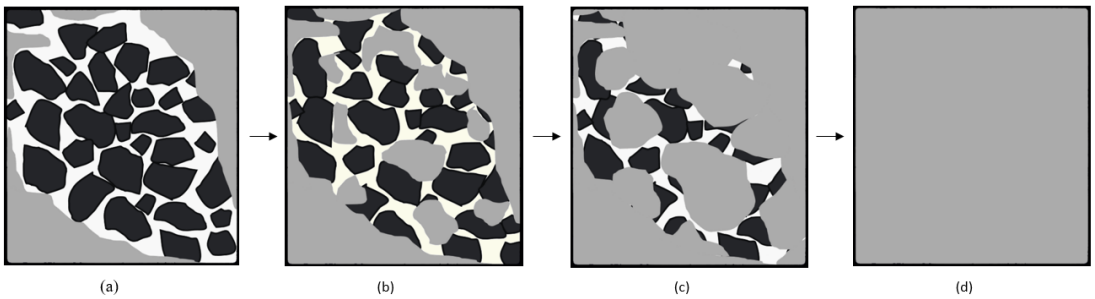

Fig. 3.4: Changes to the inner face of the mold during vibration

Whenever the cement slurry comes to the surface through air-entrapping paths, it'll create slurry spots on the surface. Further vibration leads to the development of cohesive forces between those slurry spots and creates a smooth, thin cement layer on the surface. Van der Waals forces are weak attractive forces that exist between all molecules. These forces act to bring the cement slurry droplets closer together, allowing them to merge. Capillary action occurs when the cohesive forces within a liquid, such as cement slurry, are stronger than the adhesive forces between the liquid and the mold surface. This causes the liquid to be drawn into narrow spaces, such as the gaps between the droplets, leading to their fusion. Overall, cohesive forces act to bring the individual cement slurry droplets closer together, allowing them to merge and form a continuous surface in the mold.

3.2.2 Formation of honeycombs and visual inspections

As elaborated in the previous section, the formation of a smooth, thin cement paste layer around the mold surface governs whether the honeycombing is visual to the out-

side or not. If the compaction was not done adequately, the smooth layer of cement paste will be incompleted in the mold surface and it indicates the improper compaction of concrete.

Figure 3.5 shows a case where the left face of the mix has been compacted properly, but, the right face has not been compacted up to the required level. Hence that face has an incomplete smooth layer of cement paste which highlights that there's a honeycomb. Therefore, this shows how important the occurrence of this smooth layer of cement paste is, in the identification of possible honeycombs. The construction industry has more examples of this nature, but, it lacks the discussion on the governing factors which make honeycombing visible to the outside. As a study on honeycombing in concrete structures, this study has developed a hypothesis in this regard which helps in taking actions for mitigation of honeycomb occurrences.

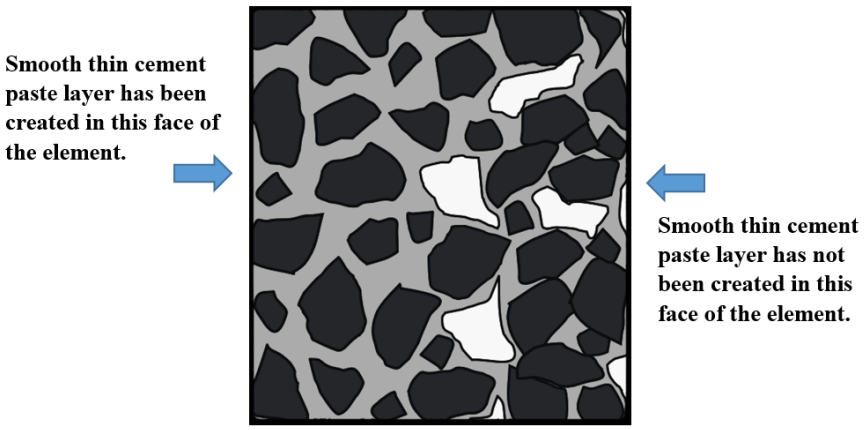

Fig. 3.5: Visibility of honeycombs and smooth layer of cement paste in the surface

3.2.3 Hidden honeycombs

There are instances where the honeycombing is not visible to the outside. What makes the honeycombing is visible? It is non other than the level of formation of the smooth, thin cement paste layer. Imagine a situation where the outer perimeter of fresh concrete is consolidated properly, but not the core. Then, there will be an unconsolidated region (a honeycomb) in the core of the concrete mix. This is not visible to the outside as the formation of a smooth thin layer of cement paste has been formed on the surface as the outer perimeter of the mix had been compacted properly. Identification of the location and severity of these hidden honeycombs is challenging. Current practices for such detections are elaborated under the chapter on Field Survey.

3.3 Importance of understanding the root cause for defects

As elaborated in this chapter, improper compaction could be the main reason for honeycombing and the improper formation of the smooth, thin layer of cement paste on the mold surface. However, that is not the only reason. Most of the time, the root causes for such defects are misunderstood as the improper compaction of fresh concrete. Therefore, proper identification of the root causes is important in avoiding the recurrence of the same defect in a project. This aspect has been addressed in depth in the next chapter. Figure 3.6 shows a case where slurry leakage leads to improper surface appearance.

Fig. 3.6: Defects due to slurry leakage

Here the mix is well compacted but, the smooth, thin layer of cement paste has been affected due to slurry leakage. Sometimes, this type of incident could be misunderstood as due to improper compaction, but it is due to poor workmanship in formwork.

CHAPTER 4

FIELD SURVEY

A field survey on honeycombs was done considering several aspects such as root causes for honeycombing, possible locations of honeycombing, and ways of mitigating such scenarios. The field survey was carried out at several local construction sites.

4.1 Defect observations

4.1.1 Defects in a concrete retaining wall due to poor workmanship in compaction of concrete.

Figure 4.1 shows a surface defect observed in the bottom of 2nd lift of 225mm thick concrete retaining wall (RW).

Fig. 4.1: Defects in a concrete retaining wall due to poor workmanship in compaction of concrete.

25mm diameter immersion vibrator had been used for compaction of concrete. The reinforcement bar detailing of the retaining wall had enough space for flow of concrete and insertion of the needle vibrator. But the needle vibrator compaction had not been carried out in a certain volume of fresh concrete; hence the proper surface finish was not achieved, and the volume left unconsolidated. The un-consolidation of the concrete is visible to the outside as smooth surface finish was not achieved in the area of concern. However, this does not mean that the defect is only on the surface. Some contractors just close these defective surfaces either by mortar or a grouting material, not knowing how far inside the unconsolidated concrete exists. At least a UPV test needs to be carried out to identify the damage inside.

4.1.2 Defects in the concrete shear wall due to reinforcement bar congestion.

It is very clear that the defect shown in Figure 4.2 is due to rebar congestion. 25mm and 40mm diameter needle vibrators had been used for the compaction of concrete.

Fig. 4.2: Defects in a concrete wall due to reinforcement bar congestion.

The defective location was congested with rebar detailing. It was observed that 25mm and 20mm diameter rebars were lapped in the same location blocking the flow of concrete. Here, the reinforcement engineer has to work on lapping locations considering the flow of concrete as well.

4.1.3 Defects in an inclined concrete column due to difficulty in compaction

Honeycombs were observed in several inclined columns of a structure as shown in Figure 4.3.

Fig. 4.3: Defects in an inclined concrete column.

25mm immersion vibrator had been used for the compaction of concrete and as per reinforcement detailing, there was enough space for inserting needle vibrator. A special feature of these rectangular columns was the inclination. Vibrator compaction

of the bottom of the inclined outer face was difficult due to this. That created defective areas.

Column lift height was 1m to avoid segregation in placing concrete. Flexible hoses had been used to place the concrete to corners under inclination. The ideal option could have been having self-compacting concrete (SCC). Thereafter, to avoid repetition of this in the remaining set of inclined columns, the needle vibrator had been attached to a steel rod and continued the compaction in unreachable corners of the column, but, that is not a standard practice.

4.1.4 Reinforcement bar congestion at a junction of four beams.

Next observation was a location where four upstand beams were connected to a column. Since the column size was also reduced at this level, some outer re-bars from the column below had been terminated. (see Figure 4.4).

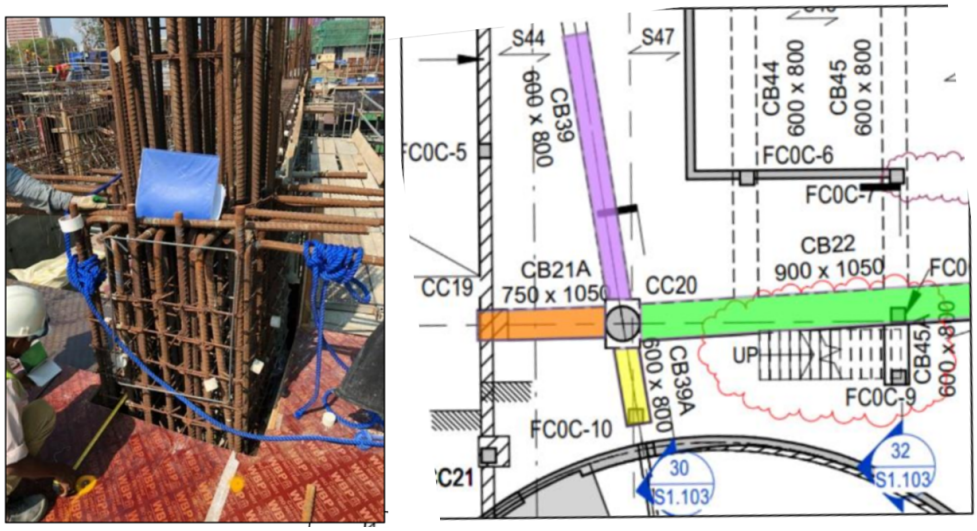

Fig. 4.4: Reinforcement bar congestion at a junction of four beams.

As per the column terminating detailing by the structural designer; terminating bars need to be bent in 'L' shape. That created the worst situation as there was no inserting space for beam rebars once the column head rebar works were done. The root cause of this issue is the impractical detailed design of reinforcement and element sizing. Secondly, the execution team should have taken this issue to the design consultants prior to the execution at site. But that needs more involvement in proper planning. The challenge here was that design consultants need to give a solution to this without affecting to the progress of the project. As a solution, the upstand beam width was increased and converted to a tapered beam, some 'L' shaped terminated bars were cut as approved by the designers and several more changes were done to beam sizing and rebar detailing. This made a considerable impact on the project's progress.

4.1.5 Surface defects due to concrete slurry leakage

This was a rectangular concrete column. Compaction had been done with a 25mm needle vibrator with no issue with re-bar congestion. But a concrete slurry leakage had taken place during the vibration due to improper mold joint preparation and resulted in creating a defective surface as shown in Figure 4.5.

Fig. 4.5: Surface defects due to concrete slurry leakage.

Sometimes, these types of defects are misunderstood as due to improper compaction. The defect can be rectified using an appropriate grout.

4.1.6 Defects due to embedded parts

Observations shown in Figures 4.6 and 4.7 were found in a shear wall where embedded parts took place.

Fig. 4.6: Defects due to embedded parts-1

Fig. 4.7: Defects due to embedded parts-2

25mm and 40mm needle vibrators had been used for compaction. Re-bar arrangement was not obstructing the compaction process, but embedded parts did, and these are the locations where moldings need to be customized. There is a possibility to have improper mold joints around the embedded parts which leads to concrete slurry leakages as well, resulting in defective surfaces.

4.1.7 Defects due to misalignment of formwork/mold

The observation shown in Figure 4.8 is a location where the formwork was misaligned to the kicker of the wall. Hence there had been a slurry leakage from the gap, and it created a defective surface.

Fig. 4.8: Defects due to misalignment of formwork/mold

4.1.8 Defects due to inadequate application of form oil

Form oil had not been applied properly to the plywood boards, hence there had been difficulty in removing the boards. In several locations, the surface cement paste had been stuck to the formwork and created defective surfaces as shown in Figure 4.9. This could be observed in several locations of the same element.

Fig. 4.9: Defects due to inadequate application of form oil

4.1.9 Segregation of aggregates was observed from the ready-mix concrete.

Fig. 4.10: Segregation of aggregates was observed from the ready-mix concrete.

As shown in Figure 4.10, at this stage (Prior to pouring concrete), the reason for segregation can be improper grading of aggregates and the differences in the specific gravity of mix constitutes. The problem with segregation is that, it cannot be physically observed as it also gives similar surface finish but weak inside.

4.1.10 Honeycombing was detected at the bottom of columns

A pre-fabricated formwork system was used for these columns. The column height was 3.5m, therefore there had been difficulty in vibrating the bottom layer of concrete from a height of 3.5m. There's a chance of segregation of concrete due to high free fall height. Well-monitored workmanship is required to attend to these challenges, and lack of attention has been the root cause for this kind of honeycombing at the bottom of the column (See Figure 4.11).

Understanding the aforementioned root causes for defects is important in preventing the recurrence of the same in the upcoming activities of a project.

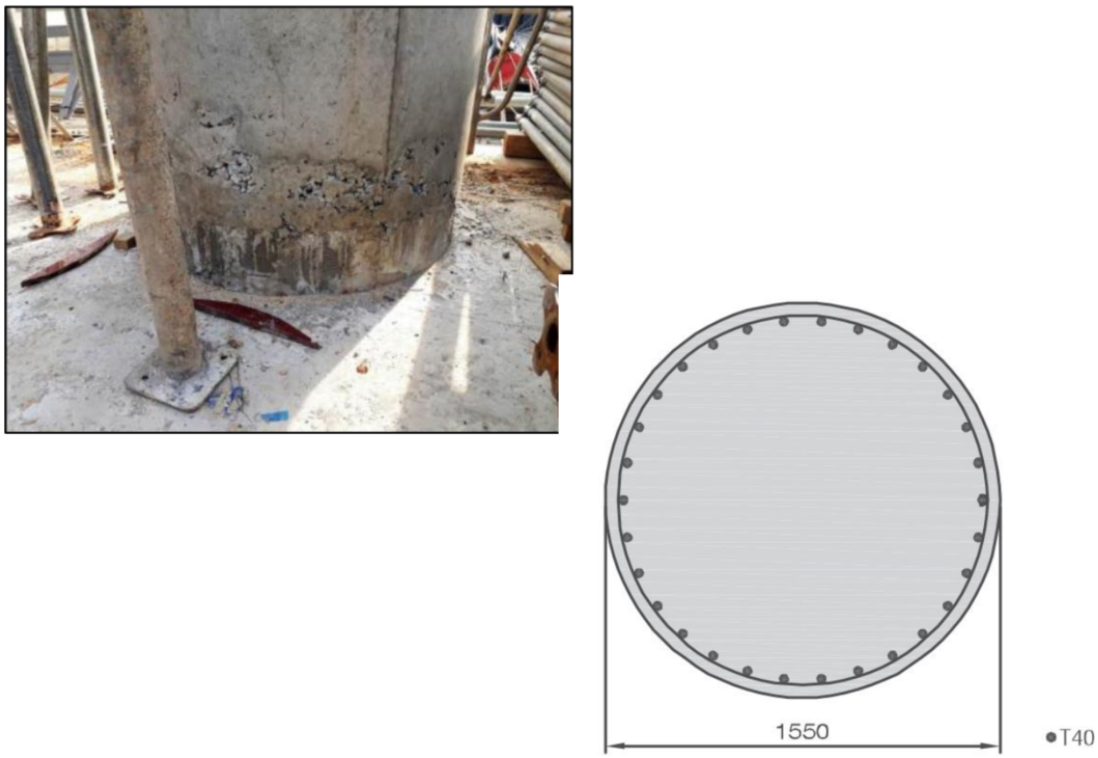

Fig. 4.11: Improper compaction at the bottom layers of 3.5m height concrete column.

4.2 Analysis of data gathered from field survey

Tables 4.1, 4.2, and 4.3 below produce a representation of some interesting data gathered from the field survey. Thirty major construction sites have been taken into consideration for this analysis.

TABLE 4.1: Number of occurrences for each root cause for honeycombing - out of 30 construction sites

SN	Root cause for honeycomb/defect	No. of cases	As a percentage
1	Due to poor compaction practices of workers	25	83%
2	Due to poor workmanship of shuttering	20	67%
3	Due to re-bar congestion	16	53%
4	Due to not applying form oil sufficiently	12	40%
5	Due to vibrator-unreachable locations	9	30%
6	Due to embedded parts in concrete	6	20%
7	Due to non-standard concrete mixes	3	10%

Consider the data in Table 4.1;

- Honeycombing due to re-bar congestion.
- Honeycombing due to unreachable locations in the complex structural elements.

- Honeycombing due to embedded parts.

Above three defective possibilities can be managed at the design stage of the structure. Improving the workmanship of the workers has to be addressed separately by showing and educating them about the standard ways of practising. Further, proper planning at the initial stages of the project has a huge impact on improving the workmanship of the workers, which means workers will not face major difficulties in handling vibrators through complex structural elements. This will be discussed later in this chapter.

TABLE 4.2: Methods used for compaction of concrete - out of 30 construction sites

SN	Method of vibration	No. of construction sites	As a percentage
1	Immersion vibrators	30	100%
2	Manual compaction	15	50%
3	External vibrators	4	13%
4	Surface vibrators	00	00%
5	Re-bar shaker	00	00%

As per Table 4.2, immersion vibrators (needle vibrators) are the most common practice in the local construction industry. Almost all the construction sites used immersion vibrators and most of the time both manual compaction and immersion vibrator compaction were used in practice.

TABLE 4.3: Methods used for honeycomb detection in construction projects - out of 30 construction sites

SN	Tests carried out for defective areas	No. of construction sites
1	UPV test	06
2	Rebound hammer test	16
3	Expert consultation	03
4	Demolition of defective element	04

As per the data in Table 4.3, defective area investigation methods in practice raise a crucial question. A common investigation test carried out is the rebound hammer test, and most of the time, the rebound hammer test was carried out for the surfaces where rectification was done. However, this method is not suitable for major defect investigations as it gives only indications on surface hardness and penetration resistance. Core defects cannot be identified through this method. Kumavat [32] has done a study on various factors affecting the results of rebound hammer test. He has elaborated that deviation in rebound index vs. compressive strength as an indication of various factors influencing the rebound index. Therefore, Kumavat [32] concludes that the effectiveness of the rebound hammer test has to be checked considering the factors affecting the results.

4.3 Improving workmanship by proper planning at initial stages: based on field survey

As discussed under field survey, proper planning at initial stages and reinforcement detailing done considering the practicality in compaction contributes to effortless improvements in workmanship.

4.3.1 Correct use of code of practice

There are some discrepancies between codes of practice for design of reinforcement and codes of practice for compaction of concrete using immersion vibrators.

First, consider BS 8110-1: 1997, Part 1: Code of Practice for design and construction. There, under clause 3.12.11.1, guidelines for minimum distance between bars is given. As per that, minimum distance required is the maximum size of coarse aggregate in concrete + 5mm [18]. This means if the maximum coarse aggregate size is 20mm, the minimum distance between bars shall be 25mm. But when it comes to compaction of concrete using immersion vibrators, it leads to major difficulties as available needle vibrator diameters range from 25mm to 90mm.

However, this issue has been addressed in BS EN 1992-1- 1: 2004, Part 1-1: General rules and rules for buildings. There, under clause 8.2 Spacing of bars, it has specifically mentioned that the spacing of bars shall be such that the concrete can be placed and compacted satisfactorily for the development of adequate bonds. Further, it has been mentioned that there should be sufficient space between the resulting columns of bars (when several layers of bars are present) to allow access for vibrators and good compaction of the concrete.

IS: 3558 1983 (Reaffirmed 2004) is an Indian Standard Code of practice for the use of immersion vibrators for consolidating concrete. Under clause 8.8 on vibrating the reinforced concrete, it recommends to make sure minimum space of 75 mm exists between the bars or groups of bars to allow the vibrator to pass freely. In local construction industry, still the British Standards are mostly used for design of reinforcement in structural elements which had given less attention for practicality in the compaction of concrete. Therefore, it is better to work on reinforcement detailing along with standards for the vibration of concrete.

4.3.2 Incorporating general details of structural drawings to special cases

As illustrated in subsection 4.1.4 of this chapter, there are some situations, where following general notes/detailing as they are, tends to create a mess. For example, there can be a general note to terminate all column re-bars by bending an anchorage length inward. But this cannot be applied directly for a heavily reinforced column as it ends

up in congestion. In such situations, execution team has to bring the issue to the designer prior to executing it at site. Most of the time, this kind of issues were taken to the designer when the work was half-way done. On the other hand, designers need to be skilful enough to foresee this type of issues at the design stage. They can make aware the execution team in advance. Usually, placements of embedded parts are done by the mechanical team of a project. They should have coordinated it with the reinforcement designers in order to avoid any kind of congestion in structural elements.

4.3.3 Points to be considered in improving workmanship related to shuttering

Most of the time, whenever a honeycombing was observed, contractors conclude it as a result of poor compaction. But the root cause can be some other reason. Understanding of root cause is important as it helps to avoid the recurrence of the same later. Defective surfaces due to concrete slurry leakage could be misunderstood as a result of poor compaction. If the root cause was understood correctly, modifications to formwork system can be arranged. Minimizing the number of joints in shuttering can be a good improvement. Then, application of form oil is also important in order to have a smooth surface finish. Most of the time, defects due to not applying form oil are misunderstood as defects due to poor compaction. If the root cause is identified correctly, the team can take necessary actions to overcome that in the next task. Use of un-damaged shutters is important to have a smooth surface. Verticality and correct alignment of formwork panels are also important to avoid honeycombing.

4.3.4 Use of self-compacting concrete and importance of experienced work groups.

For unreachable areas in structures and congested spots, self-compacting concrete can be used. However, identification of such requirements and pre-planning is important. Experienced concrete pouring groups, concrete supervisors and formwork supervisors can make a considerable impact on the outcome. There are such reputed contractors and working groups in the industry who produce concrete with fewer defects. The relationship between experienced working groups and occurring of honeycombs shall be further studied.

4.3.5 Standards used for compaction of fresh concrete

- Code of practice for use of immersion vibrators for consolidating concrete – Indian Standard IS: 3558 – 1983 (Reaffirmed 2004)
- Building construction machinery and equipment — Internal vibrators for concrete — Part 1: Terminology and commercial specifications ISO 18651-1:2011(en)
- 309-72 Standard Practice for Consolidation of Concrete (Revised 1982)

- Guide for Consolidation of Concrete Reported by ACI Committee 309 - ACI 309R-96
- Behaviour of Fresh Concrete During Vibration ACI 309.1 R-93 (Reapproved 1998)

From the above standards, Code of practice for use of immersion vibrators for consolidating concrete – Indian Standard is somewhat familiar with local construction practices. The Indian Code has mainly focused on compaction of concrete with immersion vibrator. (Which is the most practised method for compaction in Sri Lanka as well).

However, as per the discussions had with local builders, they have less or no idea about any standards for compaction, yet they are practising some correct methods as per the guidelines from the consultants and engineers. Our idea is, that these builders need to be more exposed to these standards and correct methods of practising.

4.4 Guidelines and recommendations for designers and contractors to mitigate the occurrence of Honeycombs and other Concrete Defects

4.4.1 Improving workmanship through proper planning

- **Reinforcement detailing for practical Compaction:**
  - Plan reinforcement detailing in the early stages, considering the practicality of concrete compaction.
  - Ensure that reinforcement spacing allows for adequate access for vibrators to ensure proper compaction.

4.4.2 Correct use of Codes of practice

- **Addressing discrepancies in Codes:**
  - Align the design of reinforcement spacing with standards for concrete compaction.
  - Follow BS EN 1992-1-1: 2004, which emphasizes the importance of spacing bars to allow effective concrete placement and compaction.
  - Adhere to IS: 3558 1983, ensuring a minimum of 75 mm spacing between bars to allow immersion vibrators to pass freely.

4.4.3 Incorporating general details of structural drawings into Special Cases

- **Customization of general notes for complex structures:**
  - Review and customize general reinforcement notes for specific cases to avoid congestion and compaction issues.
  - Foster proactive communication between the execution team and designers to resolve potential issues before construction begins.

4.4.4 Improving workmanship related to shuttering

- **Identification of root causes of defects:**
  - Accurately identify the root causes of defects such as honeycombing and surface irregularities.
- **Shuttering practices:**
  - Minimize the number of joints in shuttering to prevent concrete slurry leakage.
  - Ensure proper application of form oil for a smooth surface finish.
  - Use undamaged shutters and ensure correct alignment and verticality of formwork to prevent honeycombing.

4.4.5 Use of self-compacting concrete

- **Application in congested areas:**
  - Utilize self-compacting concrete in hard-to-reach and congested areas to ensure uniform compaction.
- **Importance of experienced work groups:**
  - Engage experienced concrete pouring groups and supervisors to enhance the quality of the finished concrete and reduce defects.

4.4.6 Standards for compaction of fresh concrete

- **Exposure to relevant standards:**
  - Educate builders on the standards for concrete compaction, such as IS: 3558 – 1983 and other relevant guidelines from ACI and ISO.
  - Promote adherence to these standards in local construction practices to improve the quality of compaction and reduce defects.

4.4.7 Continuous education and training

- **Workshops and Seminars:**
  - Organize training sessions for contractors and workers to familiarize them with best practices and standards in concrete compaction.
- **On-Site demonstrations:**
  - Conduct on-site demonstrations of proper compaction techniques using immersion vibrators and other tools.

CHAPTER 5

INVESTIGATION ON IMPACT FROM REINFORCEMENT ON UPV TESTS ON CONCRETE

5.1 Conventional methods used in local construction sector for defect detection in concrete structures

Rebound hammer test and ultrasonic pulse velocity (UPV) test are the most common conventional approaches in detecting the location and severity of honeycombs in structural concrete elements.

As discussed in the chapter on "Field Survey", it was found that UPV tests are mainly conducted for major doubtful locations in concrete structures. However, there's no proper investigation into the reinforcement arrangement of the area taken into consideration for the UPV test. Therefore, it's critical to understand the impact on the UPV test results due to the reinforcement arrangement of the concrete structure. Otherwise, the UPV results could be misleading or misinterpret the condition of the concrete element.

5.2 Assessing the impact of reinforcement arrangement for UPV tests

Three specimen were taken into proposed tests as shown in Figure 5.1.

- **Sketch 1**: Normal, lightly reinforced beam element without any honeycombing.
- **Sketch 2**: Lightly reinforced beam element with a 25 mm thick polystyrene layer placed in the upper half.
- **Sketch 3**: Heavily reinforced beam element with a 25 mm thick polystyrene layer, including additional reinforcement bars passing through the polystyrene layer in the longitudinal direction.

Here, expanded polystyrene (EPS) has been used to recreate honeycombs in the concrete specimen. EPS is lightweight and has a low density while blocking the concrete paste flowing through it. Honeycombs in concrete are voids with no solid material, so their density is essentially zero in the affected area. Therefore it's expected a honeycomb-like area in the concrete specimen by inserting EPS.

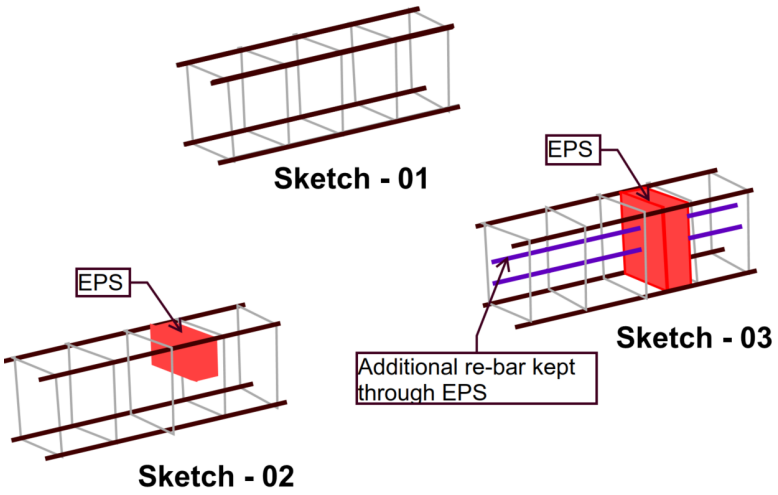

Fig. 5.1: Sketches showing reinforcement arrangement of different specimen

5.3 Specimen preparation and conduct of UPV tests

The tests were set out in a way such as to examine how impactful is the reinforcement arrangement of a concrete element for UPV tests. Figures 5.2, 5.3, 5.4, 5.5 and 5.6 below are showing specimen arrangement and conduct of UPV tests.

Fig. 5.2: Reinforcement arrangement of specimen with no honeycombs

Figure 5.2 shows the reinforcement arrangement of specimen with no honeycombs. This was used to compare the impact when there's a honeycomb in the concrete element. As elaborated earlier, dimensions were kept as 300mm x 250mm x 150mm. The 12mm diameter RE500 reinforcement bars were used with 6mm diameter mild steel stirrups as shown. Furthermore, this reinforcement arrangement has been considered a light reinforcement arrangement compared to the other specimen shown in Figure 5.4.

Fig. 5.3: Reinforcement arrangement of the lightly reinforced specimen with a honeycomb

Figure 5.3 shows the specimen with the same properties except for a known honeycombing arranged in a specified location of the concrete element. A 25mm thick polystyrene piece covering half of the cross-section of the element was used to create a deviation of the homogeneity.

Fig. 5.4: Reinforcement arrangement of the heavily reinforced specimen with a honeycomb

Figure 5.4 shows a similar specimen but with heavily reinforced concrete. Reinforcement bars going through the non-homogeneous region of the specimen make it heavily reinforced concrete as it's a possible scenario in heavily reinforced concrete elements which impacts the results of UPV tests.

Fig. 5.5: Showing lightly (LHS) and heavily (RHS) reinforcement arrangement of specimen with honeycombs

Figure 5.5 shows the lightly reinforced concrete specimen and heavily reinforced concrete specimen together. Note that additional longitudinal bars are going through the polystyrene piece in the heavily reinforced concrete element.

Fig. 5.6: Conducting the UPV test

Figure 5.6 shows how the UPV test was conducted. Cleaning of the concrete surface at the test locations is significant in ensuring good contact between the transducers and the concrete. Furthermore, a thin layer of gel, grease, or water-based substance between the transducers and the concrete surface is important in transmitting the ultrasonic waves efficiently. Instrument calibration was done prior to the testing on the beam to ensure that there were no errors in the equipment. So, time taken was measured in the Calibration rod and checked with the defined time (L=58.6 microseconds). The test was performed at Day 28 of casted concrete specimen. Grease is applied to the

contact surface to get better coupling action between the instrument and the concrete surface.

The UPV tests for these specimens were carried out for both faces as shown in Figure 5.7.

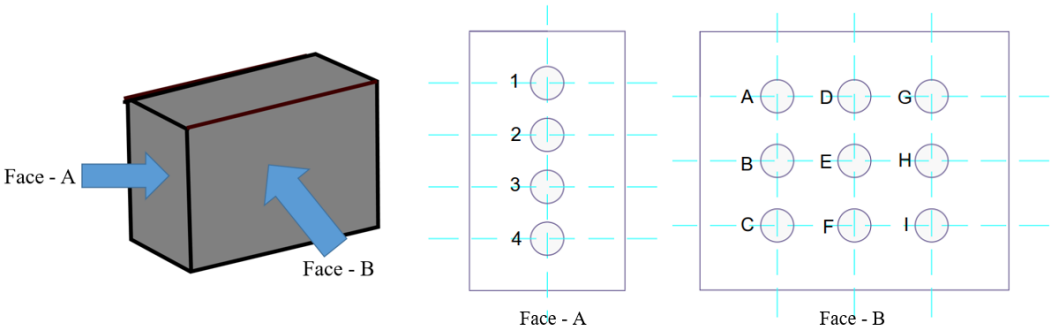

Fig. 5.7: Sketches showing faces where UPV tests were carried out

5.4 Experimental results

Tables 5.1, 5.2 and 5.3 show UPV test results for the specimen shown in figure 5.1 and test faces shown in Figure 5.7

TABLE 5.1: UPV test results for Specimen 01 - Lightly reinforced arrangement with no-honeycombs

	Specimen 01 (Sketch 01)		
	Point	**Time (µs)**	**Velocity (km/s)**
Face - A	1	79.6	3.77
	2	78.7	3.81
	3	77.8	3.86
	4	78.1	3.84
Face - B	A	39.7	3.78
	B	40.3	3.72
	C	39.9	3.76
	D	40.1	3.74
	E	39.8	3.77
	F	39.7	3.78
	G	39.6	3.79
	H	40.4	3.71
	I	39.8	3.77

TABLE 5.2: UPV test results for Specimen 02 - Lightly reinforced arrangement with honeycombs

	Specimen 02 (Sketch 02)		
	Point	**Time (µs)**	**Velocity (km/s)**
Face - A	1	96.2	3.12
	2	89.2	3.36
	3	79.3	3.78
	4	78.9	3.80
Face - B	A	38.9	3.86
	B	39.8	3.77
	C	39.2	3.83
	D	38.5	3.90
	E	40.2	3.73
	F	38.6	3.89
	G	48.4	3.10
	H	42.8	3.50
	I	39.4	3.81

TABLE 5.3: UPV test results for Specimen 03 - Heavily reinforced arrangement with honeycombs

	Specimen 03 (Sketch 03)		
	Point	**Time (µs)**	**Velocity (km/s)**
Face - A	1	98.9	3.03
	2	74.2	4.04
	3	75.8	3.96
	4	99.3	3.02
Face - B	A	38.6	3.89
	B	45.4	3.30
	C	38.9	3.86
	D	38.4	3.91
	E	39.1	3.84
	F	39.6	3.79
	G	47.9	3.13
	H	48.1	3.12
	I	47.6	3.15

5.5 Analysis of results

5.5.1 Lightly reinforced concrete with no honeycombs

If we consider the UPV test results in Table 5.1 which represents concrete elements with lightly reinforced arrangement and no honeycombs, the pulse velocities are in a certain region from 3.71 km/s to 3.86 km/s with no major deviations. This indicates that the concrete element has homogeneous properties.

5.5.2 Lightly reinforced concrete with honeycombs

Next, let's consider, the results in Table 5.2 which represents a concrete element with a honeycombing (created using polystyrene). There, the deviated area can be identified from the reduction in pulse velocity for both faces A and B. Face A and Face B are elaborated in Figure 5.7 and Figure 5.1 shows the placement of polystyrene inside the concrete element. Face A points 1 & 2 and Face B point G could be identified as per reduced pulse velocity, and it aligns with the expected output as the polystyrene piece had been placed halfway from the depth of the concrete element. Therefore, it's clear that honeycombs in lightly reinforced concrete can be identified from UPV tests.

5.5.3 Heavily reinforced concrete with honeycombs

Here, heavily reinforced concrete denotes that, there are reinforcement bars going through the honeycombed area of the element. This case was taken into consideration as there are many possibilities to create such arrangements in heavily reinforced concrete elements. In order to investigate this, the specimen was created in a way such that several reinforcement bars are going through the polystyrene piece as shown in Figure 5.1. The results show that UPV test fails to identify the surrounding honeycombs as the pulse is transmitted through the reinforcement bars. The results in Table 5.3 for Face A show that Point 2 and Point 3 observations are showing slightly high pulse velocities due to the effect of reinforcement bars parallel to the direction of the pulse. However, the observations in the perpendicular direction to the bars for the same location in Face B, shows reduced velocities. This indicates that UPV test results might be misleading whenever there are reinforcement bars going through the honeycombed areas and the measurements are taken parallel to the bars.

5.6 Conclusions

As elaborated in this chapter. UPV tests have limitations in the identification of hidden honeycombs in concrete structures. Especially, when it comes to heavily reinforced concrete, the test results can be misleading. Therefore, this study further extended

to study on an alternative approach for hidden honeycomb detection which will be discussed in the subsequent chapters.

CHAPTER 6

MATHEMATICAL APPROACH

In the previous chapter, the importance of moving into alternative approaches for the detection of hidden honeycombs in concrete structures was highlighted. As per the literature survey shown in Chapter 2, the use of vibration properties of concrete structures for damage detection is an area currently the researchers are working on. Therefore, this study focused on a novel mathematical approach in order to fill a research gap in the field of study.

Makarios [33] has presented a mathematical calculation for the identification of eigenfrequencies and mode-shapes of beams with a continuous distribution of mass and elasticity and for various conditions at support. He has used first principles for the formulations of motion Equations. Vaicatis [34] has used two-variable perturbation expansion method by simulating spatially random variables on a computer, in order to investigate characteristics of non-uniform beams. According to him, the accuracy of that method increases with higher frequencies.

Abrate [35] has shown that natural frequencies of certain non-homogeneous rods are equal to that of a uniform rod when both ends are fixed. The vibration of a beam of general shape has also been studied using the Rayleigh-Ritz approach.

There are studies on mode shape analysis of beams with arbitrarily varying cross-sections. Sohani [36] has done studies on this and has presented a mathematical approach on Euler-Bernouli and Timoshenko beams with arbitrary symmetric cross-sections. That approach can be used for different boundary conditions as well. Another study on vibration of a circular beam with variable cross sections, using differential transformation method has been carried out by Abdelgany et. al. [37].

Above studies show that there's no straight-forward method for modal analysis of non-homogeneous beams, this study has attempted to formulate an equation for modal analysis of non-homogeneous elements.

6.1 Free vibration of a homogenous system

The mathematical approach for free vibration of an ideal single-degree-of-freedom system with a homogenous distribution of mass and stiffness is well-known in the field. As elaborated by Makarios [33], the equations (6.1) and (6.2) indicate a free vibration of an ideal single degree of freedom system that has eigen-frequency = $\sqrt{\lambda}$.

$$\ddot{q}(t) + \lambda \cdot q(t) = 0 \tag{6.1}$$

$$EI_y \cdot \Phi''''(x) - \lambda \cdot \bar{m} \cdot \Phi(x) = 0 \tag{6.2}$$

Where, $\Phi(x)$ is an unknown spatial function with spatial-dimension x, and $q(t)$ is an unknown time function with time dimension t. The uniform distribution of mass is given as $m(x) = \bar{m}$, and the uniform distribution of the stiffness is given as $EI_y(x) = EI_y$, where E is the material modulus of elasticity and I_y is the section moment of inertia about the y-axis. The derivation of the equations (6.1) and (6.2) are commonly known in the field and, as such, are not explicitly presented here.

6.2 Free vibration of a non-homogenous system

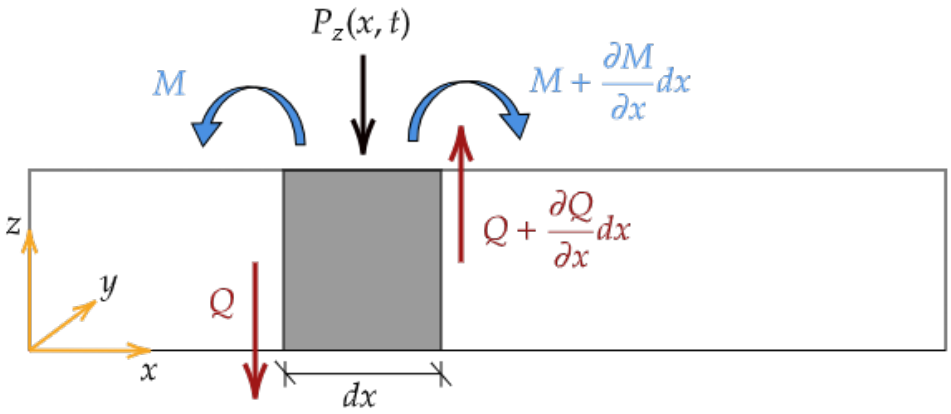

Fig. 6.1: Detailed sketch for formulation of motion equation

In Figure 6.1, the mass $m(x)$ and the stiffness $EI_y(x)$ vary with the length of the element. Hence, the element has non-homogenous properties. In this case, the equations (6.1) and (6.2) do not represent the exact modal behaviour of the system.

6.2.1 Formulation of the motion equation

In order to formulate the motion equation of the beam element with non-homogeneous properties, consider an infinitesimal part of the horizontal beam, at location x from the origin O, and the infinitesimal length of the part is dx. On this infinitesimal length, the flexural moment is $M(x,t)$ and the shear force is $Q(x,t)$ with their differential increments, while the axial force $N(x,t)$ is ignored as it does not affect the vertical beam vibration along z-axis [33].

The resulting force $P_z(x,t)$ of the external dynamic loading can be written as shown in equation (6.3), where $p_z(x,t)$ is the force per unit length.

$$P_z(x,t) = p_z(x,t) \cdot dx \tag{6.3}$$

According to D'Alembert principal, the resulting inertia force $F_a(x,t)$ is noted as shown in equation (6.4) where $u_z(x,t)$ is the unknown spatial time-function in the

direction of z-axis and $m(x)$ is the mass distribution along x-axis.

$$F_a(x,t) = (-m(x) \cdot dx) \cdot \ddot{u}_z(x,t) \tag{6.4}$$

Consider the force equilibrium of the infinitesimal part of the beam along z-axis with reference to Figure 6.1

$$\sum F_z = (Q + \frac{\partial Q}{\partial x}dx) + m(x) \cdot dx \cdot \ddot{u}_z(x,t) - P_z(x,t) - Q = 0 \tag{6.5}$$

From equation (6.3) and (6.5);

$$\frac{\partial Q}{\partial x} = p_z(x,t) - m(x) \cdot \ddot{u}_z(x,t) \tag{6.6}$$

Now, consider the moment equilibrium with reference to the weight centre of the infinitesimal part of the beam, in the direction of the y-axis (See Figure 6.1).

$$\sum M_y = M + Q\frac{dx}{2} + (Q + \frac{\partial Q}{\partial x}dx)\frac{dx}{2} - (M + \frac{\partial M}{\partial x}dx) = 0$$

$$Q = \frac{\partial M}{\partial x} \tag{6.7}$$

As per Euler-Bernoulli Bending theory, the equation (6.8) is considered for further calculations. (Where shear deformations are ignored).

$$M(x,t) = EI_y(x) \cdot \frac{\partial^2 u_z(x,t)}{\partial x^2} \tag{6.8}$$

By inserting equations (6.7) and (6.8) into equation (6.6), we can get the motion equation without damping for the considered beam element as given in equation (6.9).

$$m(x) \cdot \ddot{u}_z(x,t) + \frac{\partial^2}{\partial x^2}(EI_y(x) \cdot \frac{\partial^2 u_z(x,t)}{\partial x^2}) = p_z(x,t) \tag{6.9}$$

$$p_z(x,t) - m(x) \cdot \ddot{u}_z(x,t) = \underbrace{\frac{\partial^2}{\partial x^2}(EI_y(x) \cdot \frac{\partial^2 u_z(x,t)}{\partial x^2})}_{\text{RHS}} \tag{6.10}$$

By further simplifying the RHS of the equation (6.10);

$$\begin{aligned} &p_z(x,t) - m(x) \cdot \ddot{u}_z(x,t) \\ &\quad = EI_y(x) \cdot u_z''''(x,t) + EI_y'(x) \cdot u_z'''(x,t) + EI_y''(x) \cdot u_z''(x,t) + EI_y'(x) \cdot u_z'''(x,t) \end{aligned} \tag{6.11}$$

Here, the unknown spatial time function $u_z(x,t)$ can be written in the form of separated

variants as shown in equation (6.12).

$$u_z(x,t) = \Phi(x) \cdot q(t) \tag{6.12}$$

Where $\Phi(x)$ is an unknown spatial function and $q(t)$ is an unknown time-function. From equations (6.11) and (6.12);

$$\frac{-\ddot{q}(t)}{q(t)} = \frac{EI_y(x) \cdot \Phi''''(x) + EI'_y(x) \cdot \Phi'''(x) + EI''_y(x) \cdot \Phi''(x) + EI'_y(x) \cdot \Phi'''(x)}{m(x) \cdot \Phi(x)} \tag{6.13}$$

the left part of equation (6.13) is a time-function and the right part of the equation is a spatial function. In order to make the equation true, the two parts must be equal with a constant λ. Then, the equation is separated into two following differential equations (6.14) and (6.15).

$$\frac{-\ddot{q}(t)}{q(t)} = \lambda \Longrightarrow \ddot{q}(t) + \lambda \cdot q(t) = 0 \tag{6.14}$$

$$\frac{EI_y(x) \cdot \Phi''''(x) + EI'_y(x) \cdot \Phi'''(x) + EI''_y(x) \cdot \Phi''(x) + EI'_y(x) \cdot \Phi'''(x)}{m(x) \cdot \Phi(x)} = \lambda \Longrightarrow$$

$$EI_y(x) \cdot \Phi''''(x) + 2EI'_y(x) \cdot \Phi'''(x) + EI''_y(x) \cdot \Phi''(x) - \lambda m(x) \cdot \Phi(x) = 0 \tag{6.15}$$

Say $EI_y(x) = P(x)$;

$$P(x) \cdot \Phi''''(x) + 2P'(x) \cdot \Phi'''(x) + P''(x) \cdot \Phi''(x) - \lambda m(x) \cdot \Phi(x) = 0 \tag{6.16}$$

Equation (6.16) is a 4^{th} order linear homogeneous one, $\Phi(x)$ is the unknown spatial function in the z-direction, along the x-axis. $P(x)$ is an unknown coefficient function based on the variation of stiffness along the beam element and $m(x)$ is the other coefficient function based on the variation of mass along the beam element.

6.2.2 Applying the motion equation to a non-homogeneous element

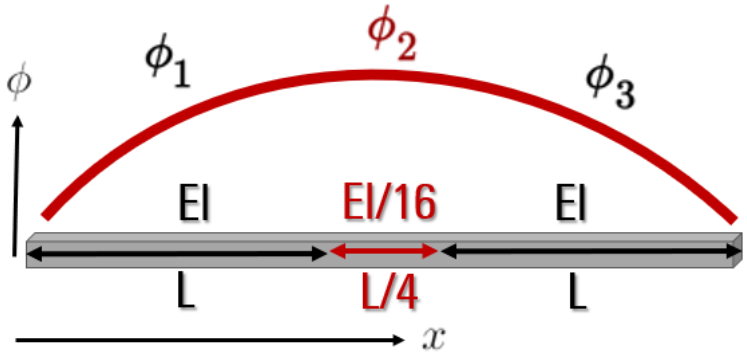

Fig. 6.2: Representing beam element with non-homogeneous properties

As shown in Figure 6.2, the beam element has a segment where stiffness and mass properties vary compared to other segments. However, the properties do not vary within a segment. For a certain segment, we have homogeneous properties. Therefore, Segment-wise functions for the mode shapes in the sample calculation are not that complex. Therefore, solving the entire equation for the mode shape by considering boundary conditions at each segment seems to be the simplest way, compared to fitting a curve for the property variation along the element using equation (6.16).

Let's say spatial functions of the three segments are $\Phi_1(x)$, $\Phi_2(x)$, and $\Phi_3(x)$.

TABLE 6.1: Property Table

	Segment 1 - Φ_1	**Segment 2 -** Φ_2	**Segment 3 -** Φ_3
Length	L	L/4	L
Stiffness	EI	$EI/16$	EI
Mass	m	m	m
Eigenfrequency	ω_1	ω_2	ω_1

As per the properties shown in Table 6.1, each segment is considered a homogeneous segment respectively. Motion equation can be applied to each segment where the length is measured in the x-direction, but, the measurements will start from zero for each segment.

Consider equation (6.16);

$$P(x) \cdot \Phi''''(x) + 2P'(x) \cdot \Phi'''(x) + P''(x) \cdot \Phi''(x) - \lambda m(x) \cdot \Phi(x) = 0$$

For a certain segment, coefficient functions of differential equation (6.16) are constants, therefore, derivatives of $P(x)$ equals to zero; hence it gives equation (6.17) as

shown below.

$$P(x) \cdot \Phi''''(x) - \lambda m(x) \cdot \Phi(x) = 0 \Longrightarrow \Phi''''(x) - \frac{\lambda \cdot m(x)}{P(x)} \cdot \Phi(x) = 0$$

$$\Phi''''(x) - \frac{\lambda \cdot m}{EI_y} \cdot \Phi(x) = 0 \tag{6.17}$$

Let's say the eigenfrequency of this single degree of freedom system as; $\omega = \sqrt{\lambda}$

$$\Phi''''(x) - \frac{\omega^2 \cdot m}{EI_y} \cdot \Phi(x) = 0 \tag{6.18}$$

Next, set the positive parameter β such as to be equal;

$$\beta^4 = \frac{\omega^2 \cdot m}{EI_y} \tag{6.19}$$

Mathematically, the general solution for the equation 6.18 is well-known and has the following form;

$$\Phi(x) = K_1 sin(\beta x) + K_2 cos(\beta x) + K_3 sinh(\beta x) + K_4 cosh(\beta x) \tag{6.20}$$

Where, K_1, K_2, K_3 and K_4 are constants. Therefore, for segment one, the general solution is considered as an equation shown in (6.21);

$$\Phi_1(x) = A_1 sin(\beta_1 x) + A_2 cos(\beta_1 x) + A_3 sinh(\beta_1 x) + A_4 cosh(\beta_1 x) \tag{6.21}$$

At $x = 0$, the displacement $u_z(0, t)$ and flexural moment $M(0, t)$ are equal to zero. By substituting these boundary conditions in equation (6.21) we get the following equation shown in (6.22) for the spatial function of segment one. Say $\beta_1 = \beta$;

$$\Phi_1(x) = A_1 sin(\beta x) + A_3 sinh(\beta x) \tag{6.22}$$

Next, consider the boundary conditions of segment two (Φ_2). Since all segments of the beam element are in motion as a single unit, the eigenfrequency (ω) needs to be equal for all segments.

Therefore, $\omega_1 = \omega_2 = \omega$, but,

$$\omega_1^2 = \frac{\beta_1^4 \cdot (EI_y)_1}{m_1}$$

$$\omega_2^2 = \frac{\beta_2^4 \cdot (EI_y)_2}{m_2}$$

Referring to Table 6.1 and considering the easiness of calculations, let's keep the mass

per unit length is same for all segments, but the stiffness is varying, therefore, $m_1 = m_2$ and $16(EI)_1 = (EI)_2$. Then, $\beta_2 = 2\beta_1 = 2\beta$.
The general solution for segment two is shown in equation (6.23);

$$\Phi_2(x) = B_1 sin(2\beta x) + B_2 cos(2\beta x) + B_3 sinh(2\beta x) + B_4 cosh(2\beta x) \tag{6.23}$$

Considering the continuity between segments, the motion/spatial properties at the end of segment 01 shall equal the motion/spatial properties at the start of segment 02.

Therefore,

- The displacement at the connecting point of segments; $\Phi_1(L) = \Phi_2(0)$
- The moment at the connecting point of segments; $EI_y \cdot \Phi_1''(L) = \frac{EI_y}{16} \cdot \Phi_2''(0)$
- The slope at the connecting point of segments; $\Phi_1'(L) = \Phi_2'(0)$
- The shear Force at the connecting point of segments; $EI_y \cdot \Phi_1'''(L) = \frac{EI_y}{16} \cdot \Phi_2'''(0)$

By substituting the above boundary conditions for segment 01 and segment 02, we get the following set of equations;

$$B_1 = \frac{5}{4} A_1 cos(\beta L) - \frac{3}{4} A_3 cosh(\beta L) \tag{6.24}$$

$$B_2 = \frac{5}{2} A_1 sin(\beta L) - \frac{3}{2} A_3 sinhh(\beta L) \tag{6.25}$$

$$B_3 = -\frac{3}{2} A_1 cos(\beta L) + \frac{5}{4} A_3 cosh(\beta L) \tag{6.26}$$

$$B_4 = -\frac{3}{2} A_1 sin(\beta L) + \frac{5}{2} A_3 sinh(\beta L) \tag{6.27}$$

The general solution for segment three is shown below by equation (6.28);

$$\Phi_3(x) = C_1 sin(\beta x) + C_2 cos(\beta x) + C_3 sinh(\beta x) + C_4 cosh(\beta x) \tag{6.28}$$

Considering the continuity between segments, the motion/spatial properties at the end of segment 02 shall equal the motion/spatial properties at the start of segment 03.

- The displacement at the connecting points of segments; $\Phi_2(L/4) = \Phi_3(0)$
- The moment at the connecting point of segments; $\frac{EI_y}{16} \cdot \Phi_2''(L/4) = EI_y \cdot \Phi_3''(0)$
- The slope at the connecting points of segments; $\Phi_2'(L/4) = \Phi_3'(0)$
- The shear force at the connecting point of segments; $\frac{EI_y}{16} \cdot \Phi_2'''(L/4) = EI_y \cdot \Phi_3'''(0)$

By substituting the above boundary conditions for Segment 02 and Segment 03, we get the following set of equations;

$$C_1 = 0.25(5B_1cos(\beta L/2) - 5B_2sin(\beta L/2) + 3B_3cosh(\beta L/2) + 3B_4sinh(\beta L/2)) \tag{6.29}$$

$$C_2 = 0.125(5B_1sin(\beta L/2) + 5B_2cos(\beta L/2) + 3B_3sinh(\beta L/2) + 3B_4cosh(\beta L/2)) \tag{6.30}$$

$$C_3 = 0.25(3B_1cos(\beta L/2) - 3B_2sin(\beta L/2) + 5B_3cosh(\beta L/2) + 5B_4sinh(\beta L/2)) \tag{6.31}$$

$$C_4 = 0.125(3B_1sin(\beta L/2) + 3B_2cos(\beta L/2) + 5B_3sinh(\beta L/2) + 5B_4cosh(\beta L/2)) \tag{6.32}$$

Furthermore, at the support end of segment Three, Displacements and Moments are equal to zero, therefore we have below two equations (6.33) and (6.34) as well.

$$C_1sin(\beta L) + C_2cos(\beta L) + C_3sinh(\beta L) + C_4cosh(\beta L) = 0 \tag{6.33}$$

$$-C_1sin(\beta L) - C_2cos(\beta L) + C_3sinh(\beta L) + C_4cosh(\beta L) = 0 \tag{6.34}$$

In order to solve for above equations, a MATLAB program was developed (See Annexes). Figure 6.3 shows the graph plots of the solutions of three segments (Φ_1, Φ_2, Φ_3).

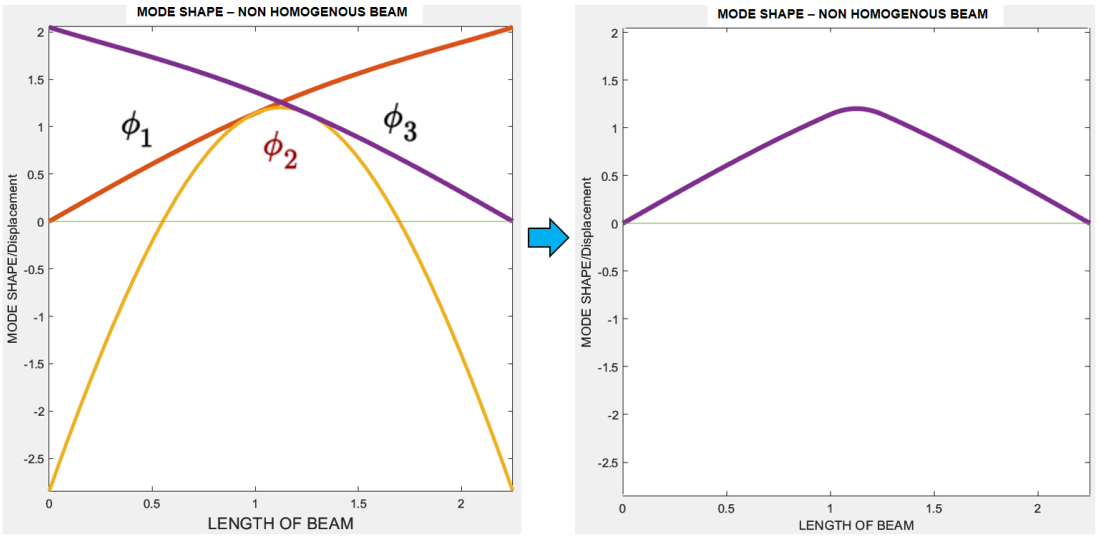

Fig. 6.3: Mode Shape of Non Homogeneous beam

Figure 6.4 shows a comparison of the mode shape with a homogeneous beam. Here, the plot in LHS is for a beam having properties of the segments One and Three of the beam we considered for the calculations. The plot in RHS shows that, due to the changes in stiffness of segment Two, the entire beam element has a different Mode Shape.

Figure 6.5 shows the plot of the mode shape difference between a normal beam and a beam having deviated stiffness properties in the middle. This is a clear indication of how the mode shape properties vary with respect to the homogeneity of the element.

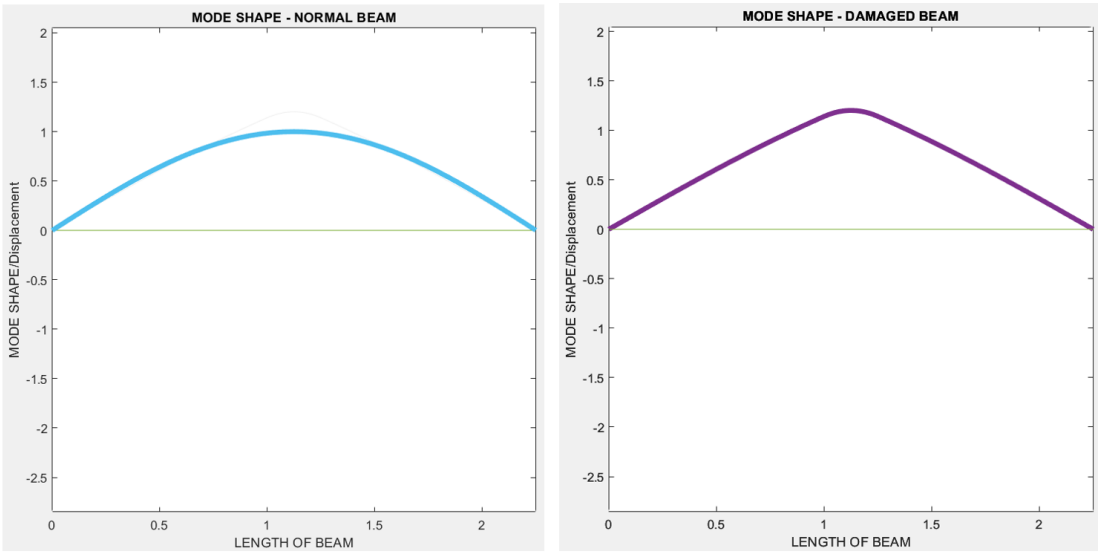

Fig. 6.4: Normal beam vs Non-homogeneous beam Mode Shape Comparison

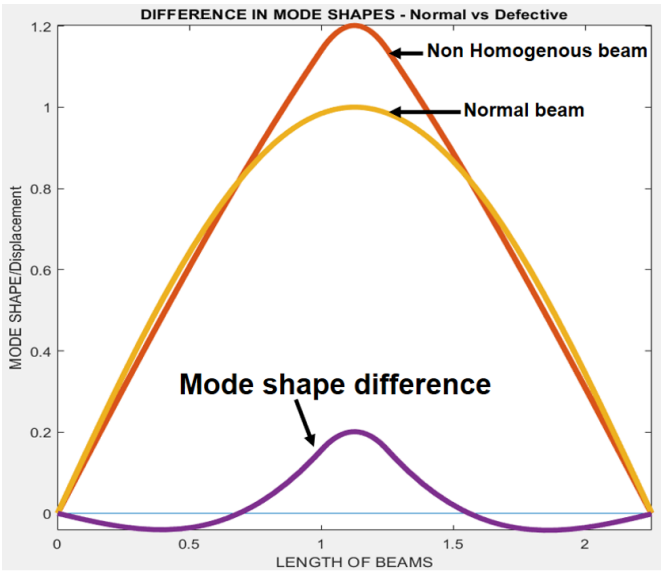

Fig. 6.5: Mode Shape Difference

6.2.3 Conclusions for mathematical approach

This study provides a novel mathematical approach for Mode Shape analysis of non-homogeneous elements. Identification of Homogeneous regions and Non-homogeneous regions in an element and implementing the mathematical model based on the continuity of the element is the key approach presented here. Furthermore, this study has

provided an equation (6.16) that is applicable to any non-homogeneous single degree of freedom system;

$$P(x) \cdot \Phi''''(x) + 2P'(x) \cdot \Phi'''(x) + P''(x) \cdot \Phi''(x) - \lambda m(x) \cdot \Phi(x) = 0$$

If the coefficient functions (i.e. Functions of change of properties) can be identified in the above equation, the equation can produce the mode shape of that non-homogeneous element. The sample calculation in this study has been provided for a beam element having reduced stiffness in a certain region, which is similar to a defective region of a structural element. Therefore, by comparing the difference in mode shapes, we can have an idea about the defect of the beam element. Furthermore, if the analysis is extended up to the comparison of mode shape curvature, more accurate identification of the location and severity of such defects can be done. If the mode shapes are available, mode shape curvature can be obtained from that.

6.2.4 Importance of mathematical approach in hidden defect detection in real-world structures

This mathematical approach or the development of mode shapes for non-homogeneous elements is for known non-homogeneity of a system. Then the question comes that, how can we use this model to observe the unknown non-homogeneity of a system? The answer is that, having this kind of a model we can analyze the behavioural patterns of mode shapes by changing parameters, so that, this can be a validation model for the experimental observations of the mode shapes of real-world structural elements. Hence, this mathematical model fills an essential gap in this study area.

CHAPTER 7

MODE SHAPE CURVATURE ANALYSIS

7.1 Introduction

In the previous section, a mathematical model was developed, in order to get the mode shape of non-homogeneous elements. In this chapter, the mode shape of non-homogeneous elements will be used to identify the defective regions in elements.

7.2 Mode shape curvature analysis - Methodology

Localized damage in a structure reduces the stiffness of the structure and that affects the mode shape of the element. It is clear that this is associated with the change in frequency as well, which shows that there is damage to the structure. However, the change in frequency only does not show the location of the damage.

Pandey et al. [5] have shown that the curvature of the mode shape is more sensitive to changes in the homogeneity of elements. This parameter is capable of locating the damages in an element as well as determining the severity of the damage.

7.2.1 Understanding the changes made to an element when there is a honeycomb

When there is a honeycomb, the defective area consists of loose particles and air voids and it does not have the expected properties of concrete. Therefore, honeycombs can be idealized as a reduction in EI (Flexural rigidity; modulus of elasticity (E) and the elements second moment of area (I))

7.2.2 Why the curvature of mode shapes are sensitive to damages

If we consider the bending equation;

$$\frac{E}{R} = \frac{M}{I} = \frac{f}{y} \tag{7.1}$$

$$\frac{1}{R} = \frac{M}{EI} \tag{7.2}$$

Where $\frac{1}{R}$ is the curvature of the location considering.

Whenever there is a reduction in EI, the curvature of that point increases [5]. This shows that there is a relationship between the curvature of a certain location and the Flexural Rigidity of that point. In our analysis, for the idealization of honeycomb, we have considered the reduction of E value while keeping I constant. By considering

the difference in curvature of defective and normal elements along their length, we can have an idea of the damaged location and the severity of the damage.

We know that there are own mode shapes for every element. If the mode shape of an element can be identified, curvature related to that mode shape can be calculated. The knowledge related to the development of equations for mode shapes is already established. Therefore, through mode shape curvature analysis, we can observe the location and severity of honeycombs in structural concrete elements.

7.2.3 Formula used for the determination of the curvature for a given function

Curvature; $k = \frac{1}{R}$ and y is the mode shape along the x-direction. See equation 7.3

$$k = \frac{\frac{d^2(y)}{dx^2}}{[1 + (\frac{d(y)}{dx})^2]^{\frac{3}{2}}} \tag{7.3}$$

If the function of the mode shape y is available, we can derive the mode shape curvature function for that based on the equation 7.3.

7.2.4 Mode shape curvature of a given mode shape

Consider the mode shape of the element discussed under the mathematical approach in Chapter 6. See Figure 7.1 below. It shows the mode shapes of the homogeneous beam and the non-homogeneous beam. From the mode shapes itself, it is clear that there is a deviation in the non-homogeneous beam element compared to the normal beam element. The functions of the mode shapes for both cases were taken from the MATLAB program and the curvature plots of them were derived using the equation 7.2. Figure 7.2 shows the curvature of mode shapes for both cases respectively. As elaborated in the previous chapter, the stiffness of one beam (in the middle region) deviated from the other regions of the beam. That change can be observed from the plots of the mode shape curvature of that beam (See Figure 7.2).

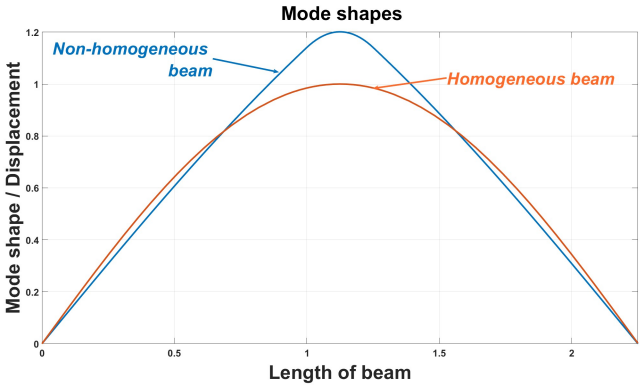

Fig. 7.1: Normal beam Vs Non-homogeneous beam Mode Shape Comparison

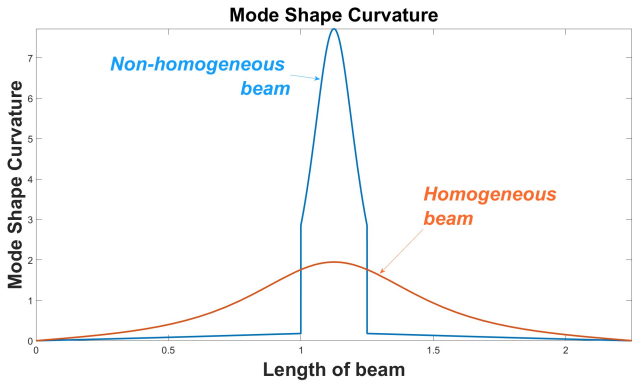

Fig. 7.2: Normal beam Vs Non-homogeneous beam Mode Shape Curvature Comparison

7.2.5 Difference of Mode shape curvatures

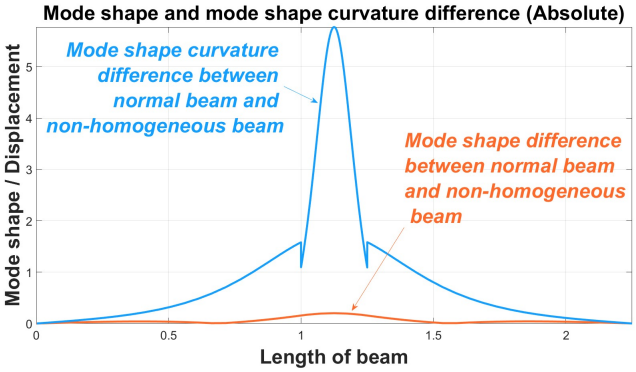

Fig. 7.3: Normal beam Vs Non-homogeneous beam Mode Shape Curvature Difference Comparison

See Figure 7.3, which shows the absolute difference of mode shapes between the normal beam and non-homogeneous beam in blue color and the difference in mode shape curvature in orange color. It is clear that the mode shape curvature is more sensitive in detecting homogeneity deviations of elements.

As shown in Figure 7.4, the middle $L/4$ of the beam is having deviated stiffness of $EI/16$, where L is the total length of the beam element, while the normal beam element has a stiffness of EI throughout the entire beam element. Therefore, we can see a considerable change in the difference in mode shape curvatures between normal and non-homogeneous beam elements in the mid-region of the beam.

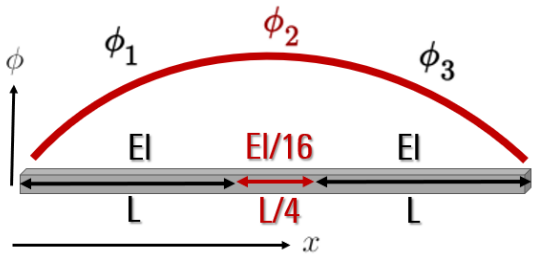

Fig. 7.4: Non-homogenity properties of beam element

7.3 Mode shape curvature analysis

As discussed in the previous section, mode shape curvature is a good parameter in identifying defective/non-homogeneous regions in a concrete beam element. Further analysis in this regard has been carried out focusing on the below points.

- Severity of the non-homogeneity and mode shape curvature
- Extent of the non-homogeneity region and mode shape curvature
- Identification of exact defective region based on mode shape curvature analysis

7.3.1 Methodology

Figure 7.5 shows the methodology for the analysis. SAP2000 software was used for developing finite element models. The defective region was created by introducing certain regions of the beam with reduced stiffness in material properties. Then, the mode shape along the beam length was extracted by taking the displacements of the nodes of the finite element model. Thereafter, in order to get the variation of the mode shape curvature along the beam length, the mathematical function of the mode shape was developed and extracted the mode shape curvature from equation 7.3. MATLAB software was used for the calculations and the code is given in the Appendix A.

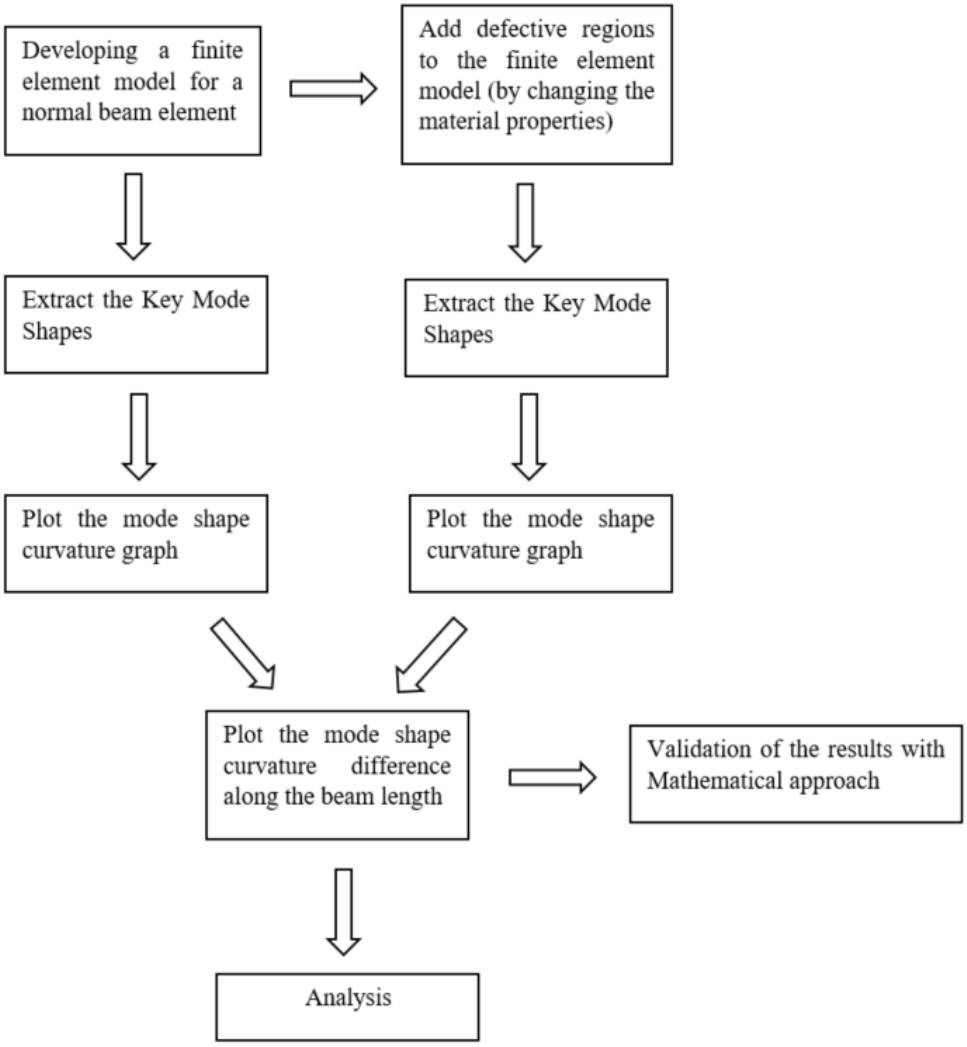

Fig. 7.5: Flow chart showing methodology for mode shape curvature analysis

7.3.2 Development of the finite element models

SAP2000 software was used to develop the finite element model. A 6m long 150mm x 300mm beam was taken into consideration. 600 segments and, 601 nodes were utilized in the finite element model (See Figure 7.6) in order to get the displacement readings at each node. The displacements at each node were recorded and used to fit a curve for the data using MATLAB. An example is shown below. The material properties were used as usual homogeneously.

Mode shape 4 of the beam is considered. The nodal displacements (in the vertical direction (z) of 601 points are as follows;

$z = [0 \quad -0.018386 \quad -0.036771 \quad \dots \quad \dots \quad 0.018386]$

The nodal points are along the horizontal direction x

$x = [1 \quad 2 \quad 3 \quad \dots \quad \dots \quad 601]$

Fig. 7.6: Nodes in Finite Element Model, total 601 nodes for 6m long beam element

Curve fitting was done for z against x with the help of MATLAB software.

Sum of Sine Curve Fit (sin8)

f(x) = a1*sin(b1*x+c1) + a2*sin(b2*x+c2) + a3*sin(b3*x+c3) + a4*sin(b4*x+c4) + a5*sin(b5*x+c5) + a6*sin(b6*x+c6) + a7*sin(b7*x+c7) + a8*sin(b8*x+c8)

Coefficients and 95% Confidence Bounds

	Value	Lower	Upper
a1	1.7558	1.6034	1.9081
b1	0.0105	0.0099	0.0110
c1	3.1208	2.9312	3.3103
a2	0.0001	-12.4431	12.4432
b2	0.0264	-17.2694	17.3223
c2	-1.9683	-1.1627e+05	1.1626e+05
a3	0.0001	-27.6137	27.6139
b3	0.0309	-1.8709e+03	1.8709e+03
c3	-0.8398	-6.0915e+05	6.0914e+05
a4	0.0001	-28.6899	28.6901
b4	0.0383	-2.5156e+03	2.5156e+03
c4	-0.0641	-7.9266e+05	7.9266e+05
a5	0.0001	-2.2626	2.2628
b5	0.0504	-1.9740e+03	1.9741e+03
c5	-0.6837	-6.0879e+05	6.0879e+05
a6	0.0001	-8.9308	8.9309
b6	0.0603	-983.0079	983.1284
c6	-0.5640	-3.0076e+05	3.0076e+05
a7	0.0000	-1.8783	1.8784
b7	0.0711	-186.3731	186.5153
c7	-0.7361	-5.6755e+04	5.6753e+04
a8	0.0000	-0.0969	0.0970
b8	0.0832	-7.4141	7.5805
c8	-1.2670	-2.2714e+03	2.2688e+03

Fig. 7.7: Details of the curve fitting - sum of sine - 08 Terms (MATLAB software)

Figure 7.7 shows the data of the curve fitting carried out with MATLAB, for the nodal displacements taken from the finite element model. The accuracy of the curve fitting is important in carrying out further analysis. Furthermore, the curve fitting function will be used to generate the mode shape curvature. Figure 7.8 shows the fitted curve.

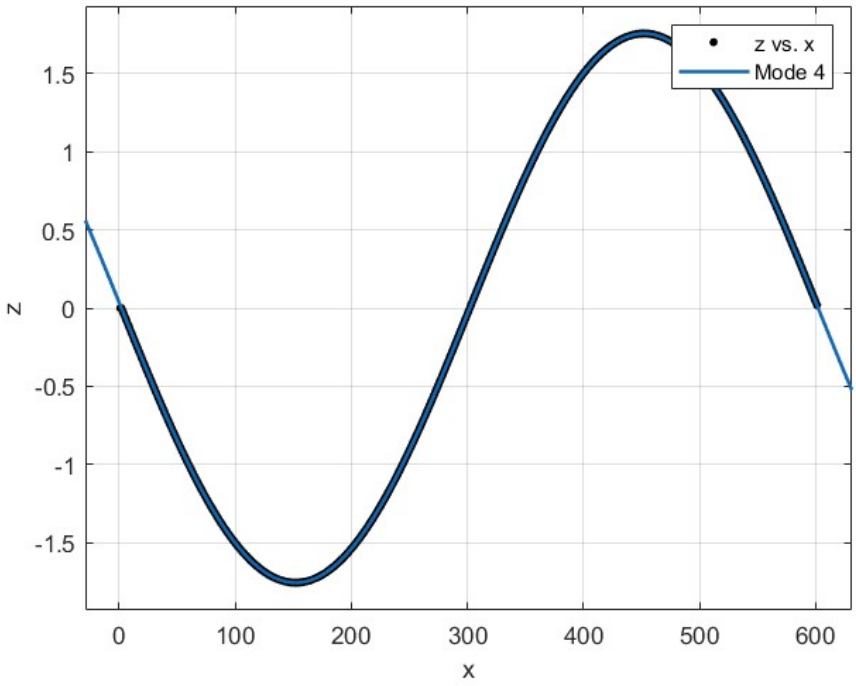

Fig. 7.8: Curve fitted plot for Mode 4 - sum of sine - 08 Terms (MATLAB software)

7.3.3 Extracting the mode shape curvature

As elaborated earlier, when the function of the mode shape is available, it is possible to get the function of the mode shape curvature by using formula 7.4, where y is the function of mode shape and k is the curvature.

$$k = \frac{\frac{d^2(y)}{dx^2}}{[1 + (\frac{d(y)}{dx})^2]^{\frac{3}{2}}} \tag{7.4}$$

MATLAB software was used to generate the plot of the mode shape curvature. The code used is given in the Annexures. The Mode Shape Curvature plot is shown in Figure 7.9 together with the respective mode shape.

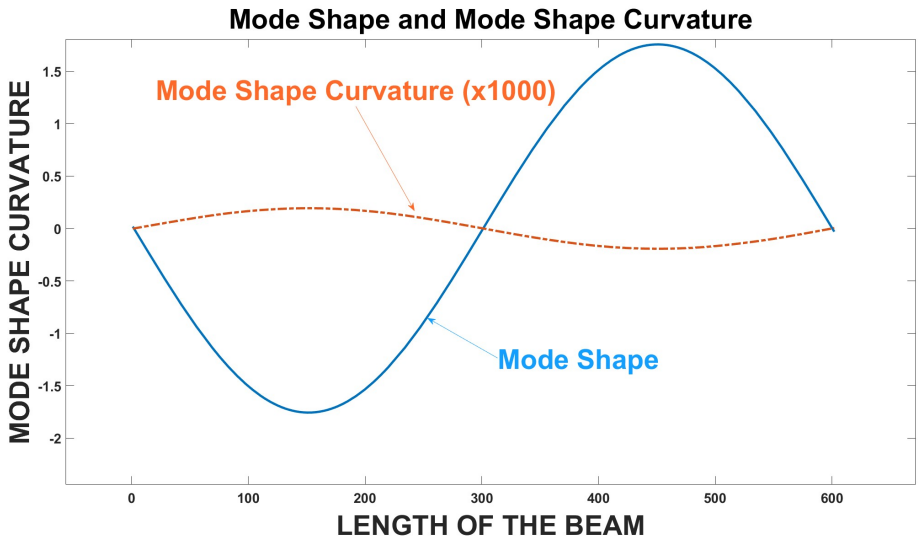

Fig. 7.9: Mode shape and Mode shape curvature plot together

For the easiness in visibility together with the mode shape, mode shape curvature values were multiplied by 1000 times and scaled up. This procedure was followed for further analysis and comparison of the mode shape curvature changes.

7.4 Detection of honeycombs with mode shape curvature analysis

Defective regions are introduced to the Finite Element Model by reducing the stiffness of certain areas by 10 times the usual stiffness. In this case, let's provide reduced stiffness from nodes 200 to 205 and 450 to 455, which will create two separate defective regions as shown in Figure 7.10.

Fig. 7.10: Simulated defective locations in the beam

Figure 7.11 shows the curve, fitted with the sum of sines (8 terms), and, slight deviations of the defective regions in the mode shape can be identified from the graph. Nodes 200-205 and nodes 450-455 are the regions where the reduced stiffness prop-

erties are introduced. Following similar steps shown previously, we can generate the mode shape curvature plot along the beam length.

The next task is to get the mode shape curvature difference between both cases (i.e. normal beam and the defective beam). The plot of the mode shape curvature difference will show the regions of deviated stiffnesses clearly.

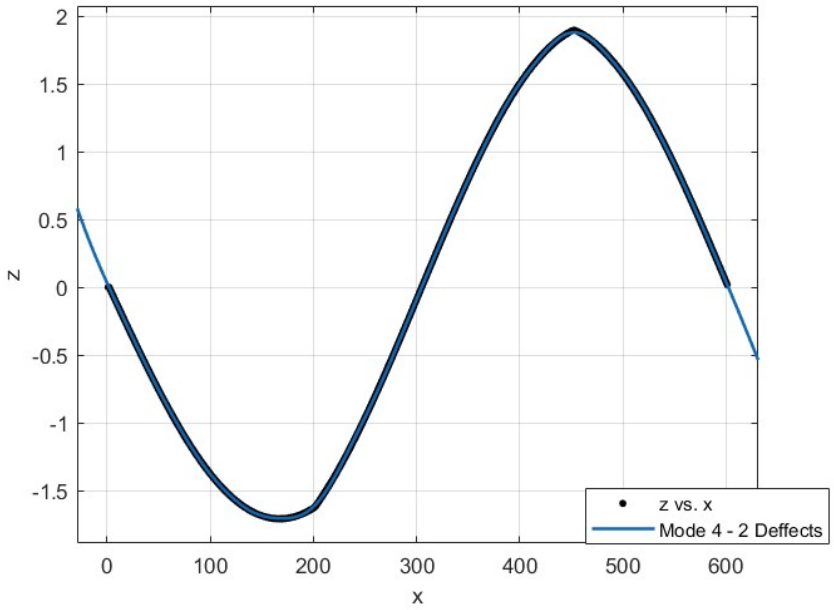

Fig. 7.11: Curve fitted plot for Mode 4 with two defective locations: 200-205 and 450-455

7.4.1 Feasibility of using the same simulation to assess the defects within a given section

This has not been assessed in this study as it considers the average reduction of the stiffness across a section. Furthermore, the objective is to identify the hidden damage location in a longitudinal direction of the element. Therefore the indications will interpret that there is a defective region at this point when measured along the element. Further investigations can be done thereafter, to examine the variation of the defective regions across a section.

7.4.2 Mode shape curvature analysis

See Figure 7.12 which shows the curvature of the mode shape of the beam, the mode shape curvature itself highlights the reduced defective regions in nodes 200-205 and 450-455.

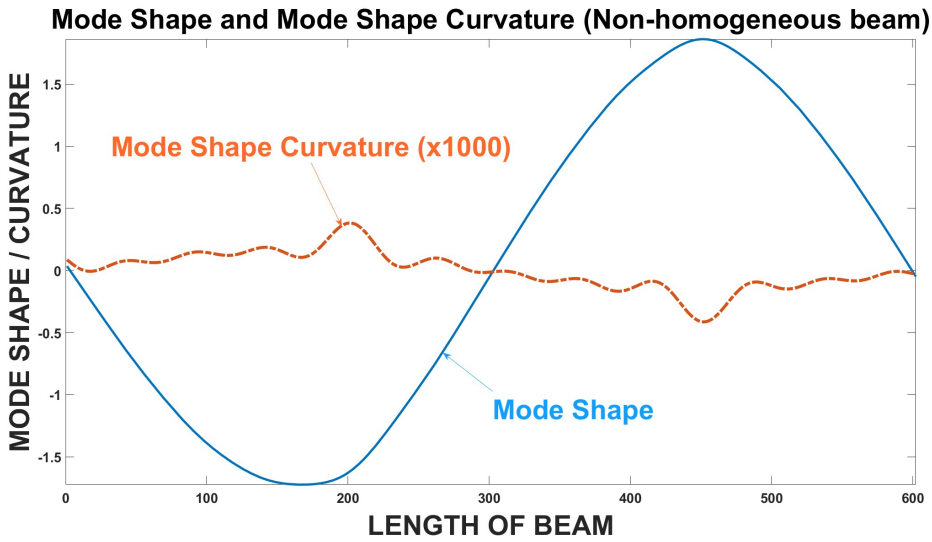

Fig. 7.12: Mode shape and Mode shape curvature plots with two defective locations: 200-205 and 450-455

However, the comparison of mode shape curvature differences between a normal beam and a defective beam will provide a more sensitive representation of the damaged locations along the beam. Plots related to this are shown in Figure 7.13.

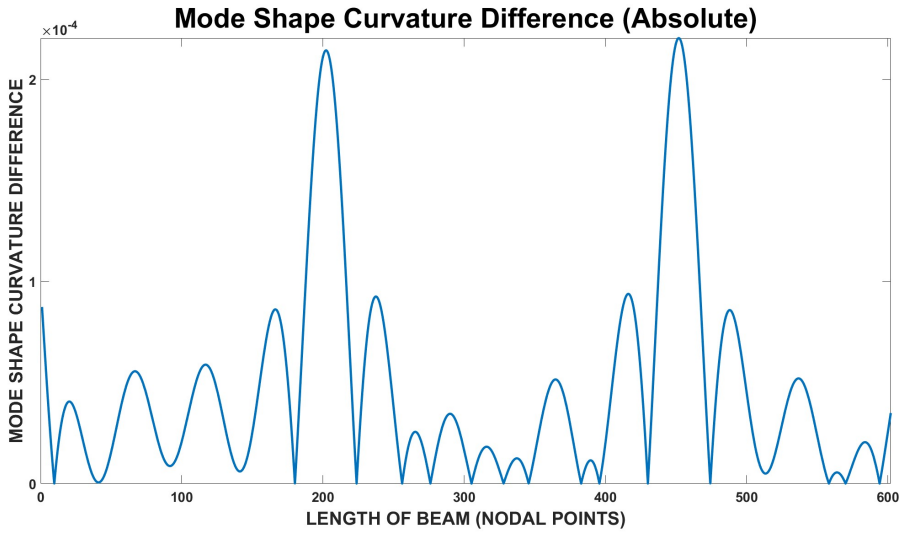

Fig. 7.13: Mode shape curvature difference between normal beam and damaged beam: 200-205 and 450-455

Figure 7.13 clearly highlights that the defective regions are in the nodal points 200-205 and 450-455. Therefore, we can say that the mode shape curvature difference between a normal beam element and a defective beam element is a good parameter to identify the defective locations in an element.

Can't we use the difference in mode shapes (displacements) to detect the defective locations? Figure 7.14 shows the plot of mode shape difference where no clear signs for detection of defective locations. Therefore, it shows how important is the mode shape curvature analysis in the detection of construction defects like hidden honeycombs.

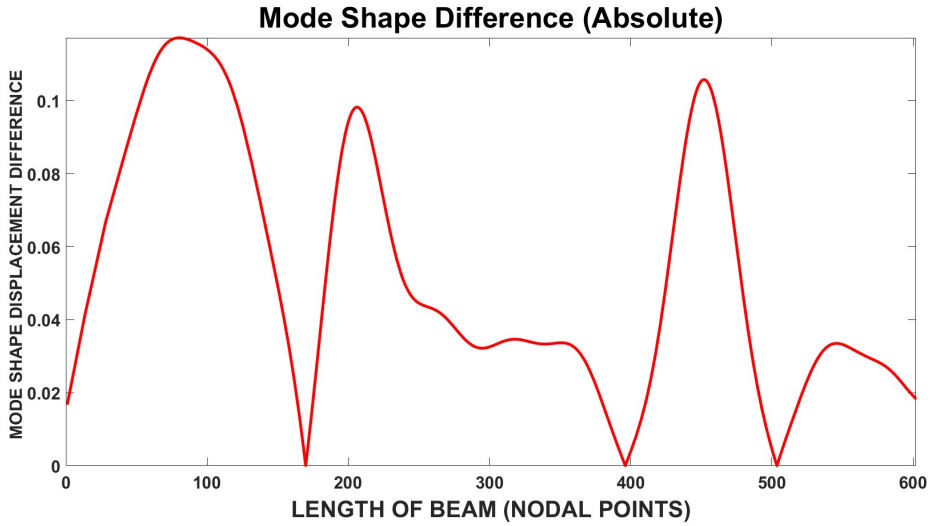

Fig. 7.14: Mode shape difference between normal beam and damaged beam: 200-205 and 450-455

7.5 Impact on the mode shape curvature analysis when the severity of the damage is varying.

For this analysis, the impact will be checked by changing the stiffness property of the element.

The severity of the damage varied changing the stiffness of the material such as a percentage of the initial E (Elasticity) value of the material. (i.e 90% of E, 80% of E, 70% of E, ... , 20% of E, 10% of E). The number of Nodes used for the Finite Element Model is 601 for a length of 6m. Therefore the distance between two nodes was 0.01m. The defective regions are from nodes 200-205 and nodes 450-455.

Figure 7.15, 7.16, 7.17 and 7.18 show the sensitivity of mode shape curvature difference plots in detecting defective regions on different severities of the defect. (i.e 90%, 70%, 50% and 90% of severity respectively). It clearly shows that the mode shape extracted from the finite element model produces high sensitivity in detecting defects more than 50% of damage intensity. However, this can be further addressed by improving the finite element model.

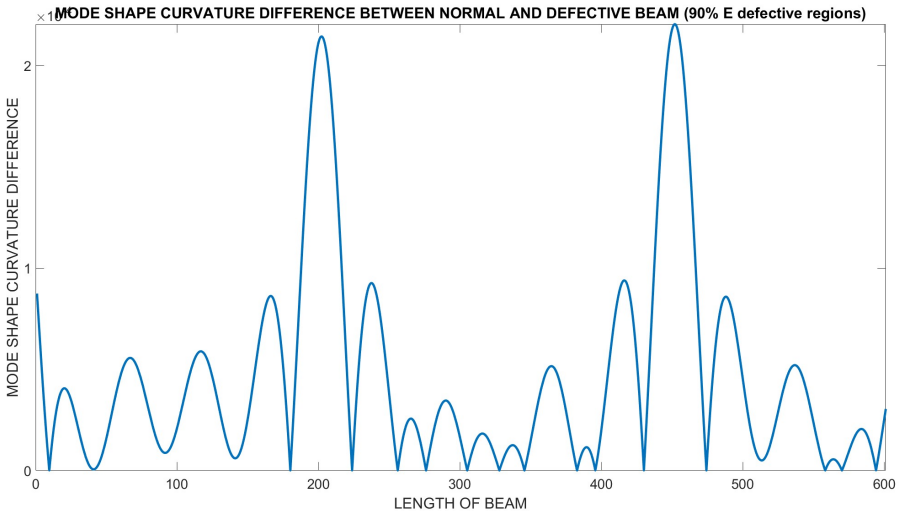

Fig. 7.15: Mode shape curvature difference between normal beam and 90% of E damaged beam; Number of Nodes = 601, damaged regions = Nodes 200-205 and 450-455

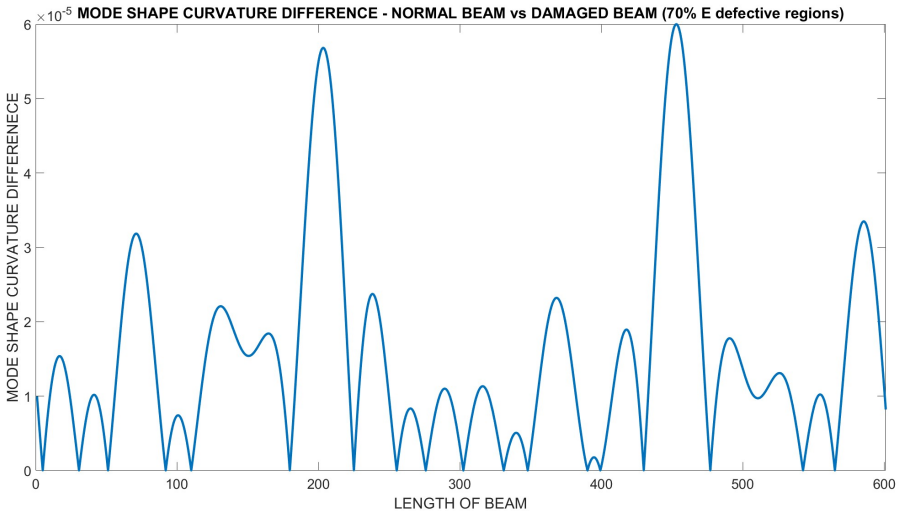

Fig. 7.16: Mode shape curvature difference between normal beam and 70% of E damaged beam; Number of Nodes = 601, damaged regions = Nodes 200-205 and 450-455

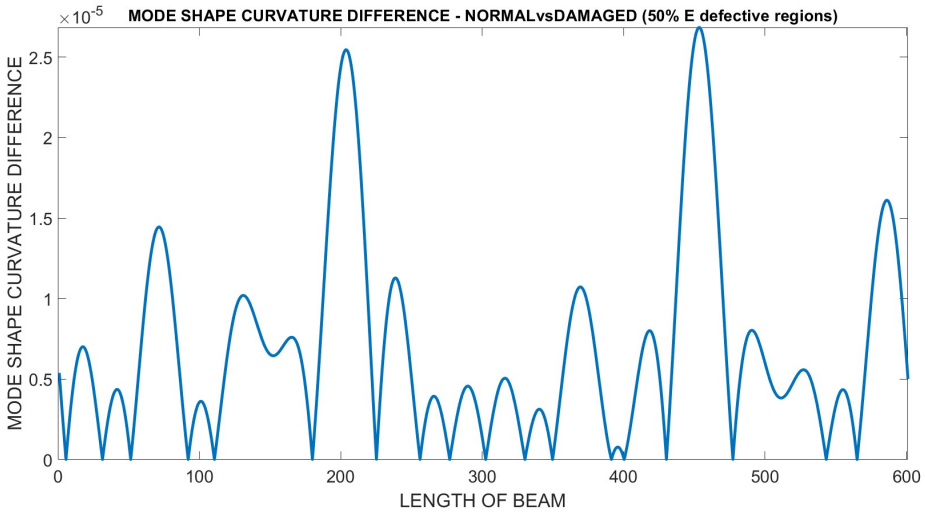

Fig. 7.17: Mode shape curvature difference between normal beam and 50% of E damaged beam; Number of Nodes = 601, damaged regions = Nodes 200-205 and 450-455

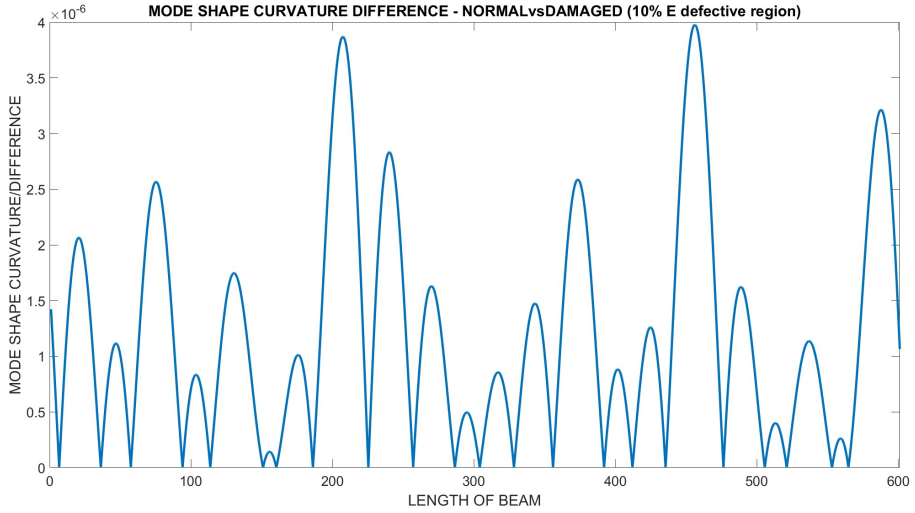

Fig. 7.18: Mode shape curvature difference between normal beam and 10% of E damaged beam; Number of Nodes = 601, damaged regions = Nodes 200-205 and 450-455

Figure 7.19 shows the comparison of different intensities together in one graph.

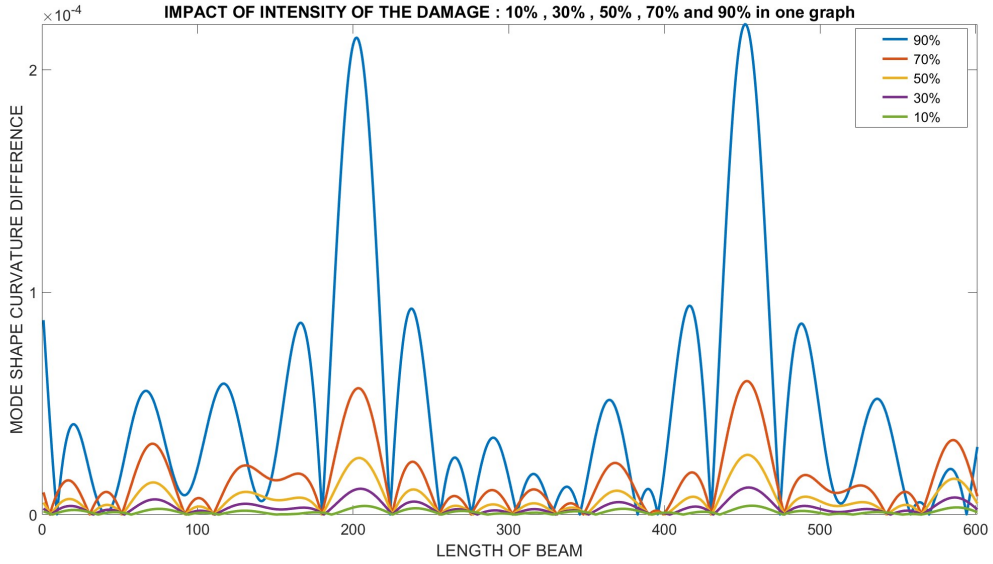

Fig. 7.19: Mode shape curvature differences for different intensities of damage

7.6 Low-intensity damage detection

7.6.1 Improving the finite element model in order to detect low-intensity damage regions in an element.

The finite element model used so far had 601 nodes only for the entire beam length of 6m. Let's increase it to 1201 nodes.

Figure 7.20 and Figure 7.21 show that the 50% damage scenario and 90% damage scenario are sensitive in damage detection when the number of nodes in the finite element model were doubled. (from nodes 601 to 1201). As elaborated in previous sections, the sensitivity in mode shape curvature difference plots depends on the process followed in extracting the mode shape plot, fitting a function to the mode shape plot, and conversion of the mode shape function to the mode shape curvature plot.

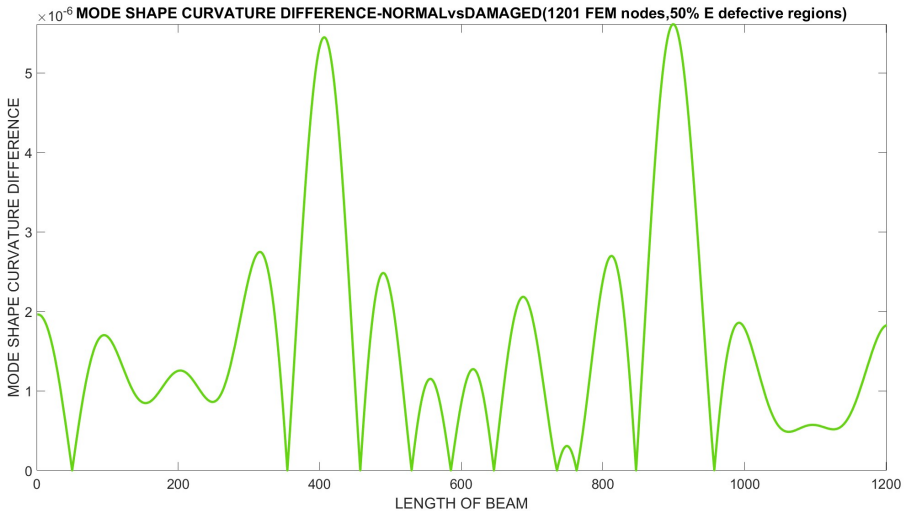

Fig. 7.20: Mode shape curvature difference between normal beam and 50% of E damaged beam; Number of Nodes = 1201, damaged regions = Nodes 400-410 and 900-910

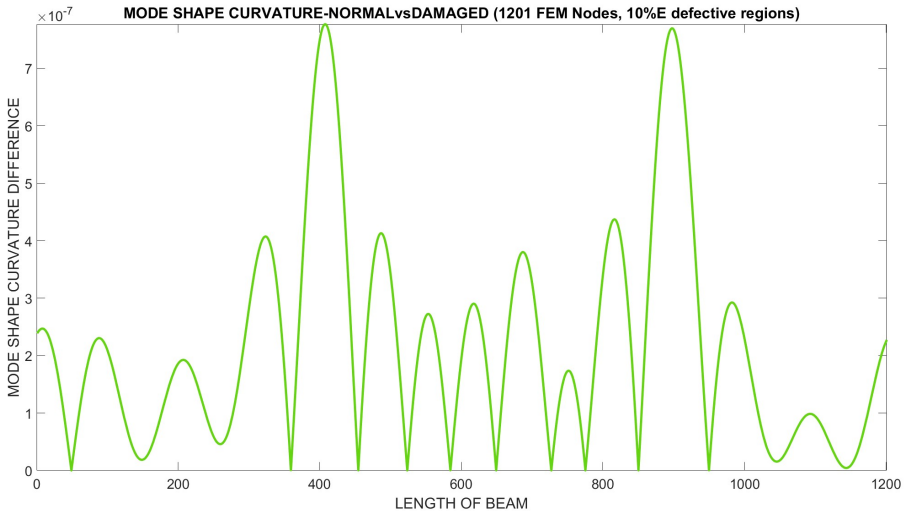

Fig. 7.21: Mode shape curvature difference between normal beam and 10% of E damaged beam; Number of Nodes = 1201, damaged regions = Nodes 400-410 and 900-910

7.6.2 Limitations in detecting damages when the damage intensity is very low

Figure 7.22 shows the plot of mode shape curvature difference for an element when there are 05% of intensity defective regions. The plot is not responsive enough to detect the defective locations. Therefore, the FEM has been improved by doubling the number of nodes again from 1201 to 2401 (See Figure 7.23). Yet, the mode shape curvature difference shown in Figure 7.23 does not highlight the defective regions.

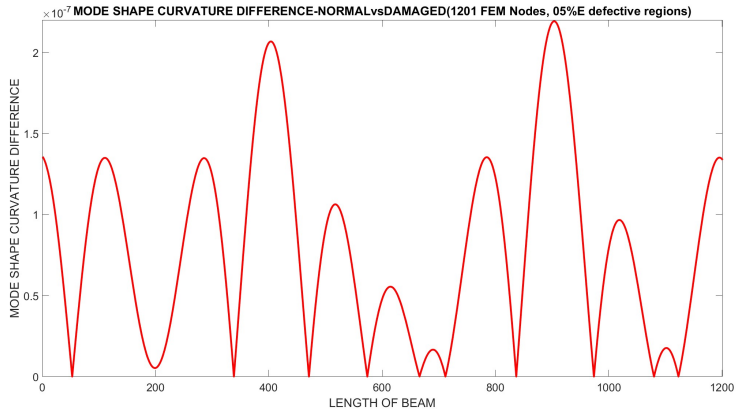

Fig. 7.22: Mode shape curvature difference between normal beam and 05% of E damaged beam; Number of Nodes = 1201, damaged regions = Nodes 400-410 and 900-910

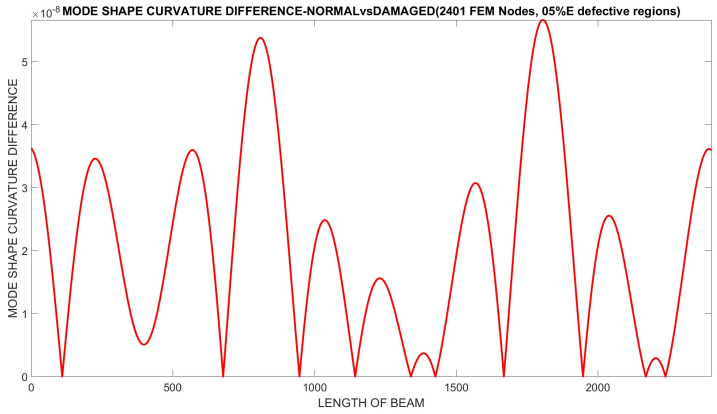

Fig. 7.23: Mode shape curvature difference between normal beam and 05% of E damaged beam; Number of Nodes = 2401, damaged regions = Nodes 800-820 and 1800-1820

Based on the above plots, it's clear that further increments in the number of nodes do not help to detect the 05% defective regions. The reason for this is the level of accuracy in fitting a curve for the mode shape node displacement data. For all the above scenarios, the "Sum of sines" method has been used with 8 terms and that is

accurate enough to detect defective regions up to a damage intensity of 10% only. For damage intensities less than 10%, that approach is not sufficient even though the FEM models were improved. Deviations between Nodal displacement points of mode shape and the Fitted Curve are shown in Figure 7.24.

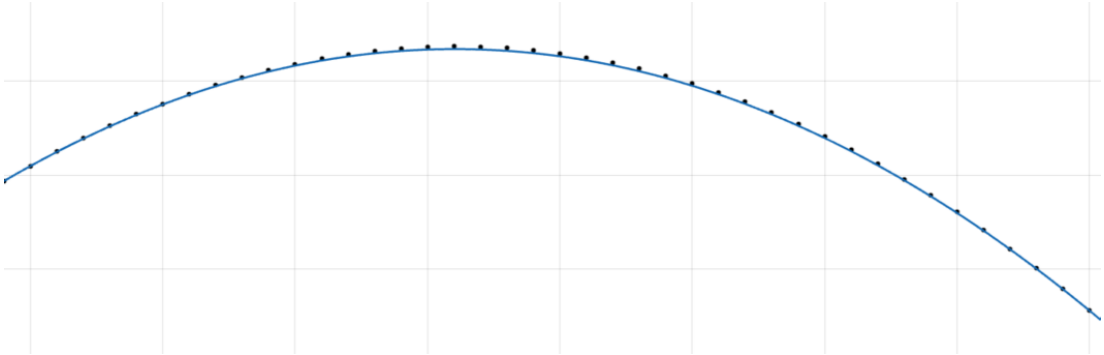

Fig. 7.24: Deviations between Nodal displacement points of mode shape and the Fitted Curve

7.7 Impact on change of mode shapes

All the previous examples were based on Mode shape 4 of the elements.

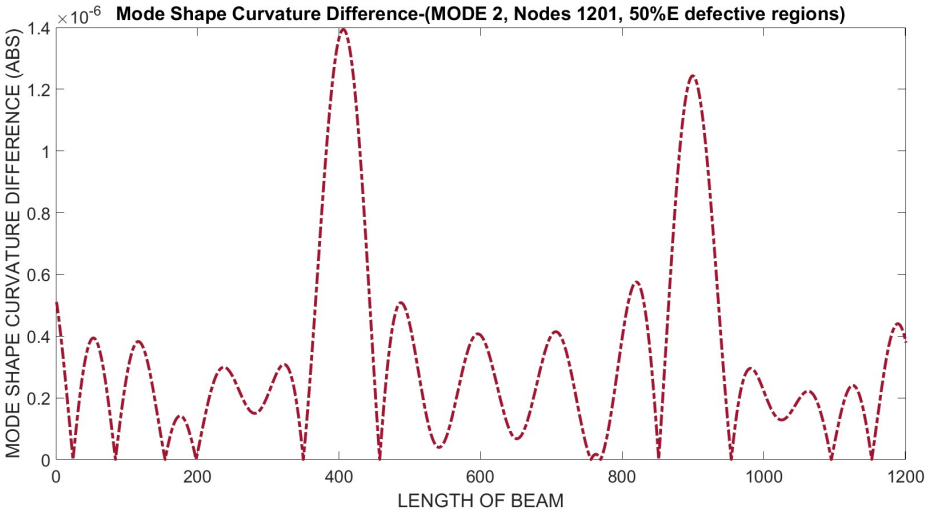

Fig. 7.25: Mode shape - 2 ; curvature difference between normal beam and 50% of E damaged beam; Number of Nodes = 1201, damaged regions = Nodes 400-410 and 900-910

Figure 7.25 is the plot of the mode shape curvature difference for Mode Shape 2. Regardless of the mode shape 2 or 4, the defective regions could be identified although the levels of identification are different.

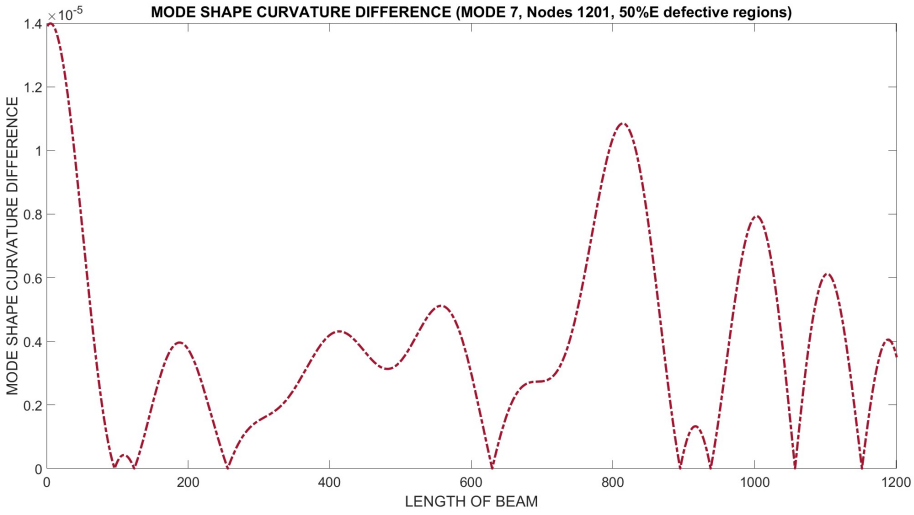

Fig. 7.26: Mode shape - 7 ; curvature difference between normal beam and 50% of E damaged beam; Number of Nodes = 1201, damaged regions = Nodes 400-410 and 900-910

Figure 7.26 shows the mode shape curvature difference for mode shape 7 and it does not clearly show the defective regions. Furthermore, the mode 2 plot and mode 4 plot are more strong compared to the mode 7 plot in detecting defective regions. This shows that the initial mode shapes are more sensitive in detecting defects when this method was followed. In other words, the method is successful for lower frequencies.

7.8 Different mode shapes and mode shape curvature analysis

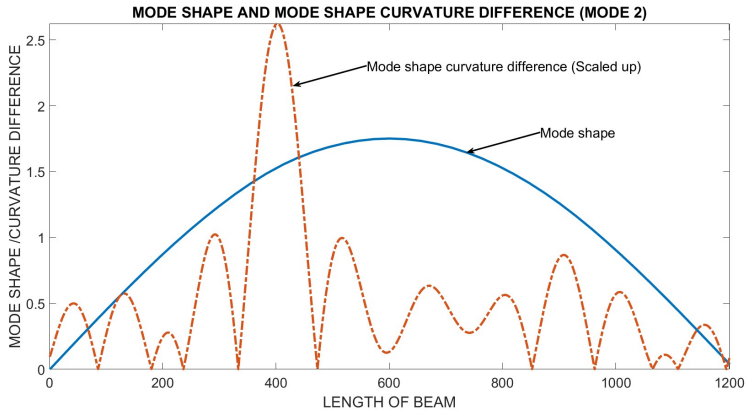

Fig. 7.27: Mode shape - 2 ; curvature difference between 70% damaged (400-410) and 50% damaged (900-910) beams

As observed from Figure 7.27 and Figure 7.28, when there are defective regions in different intensities, the mode shape curvature analysis can provide the severity levels

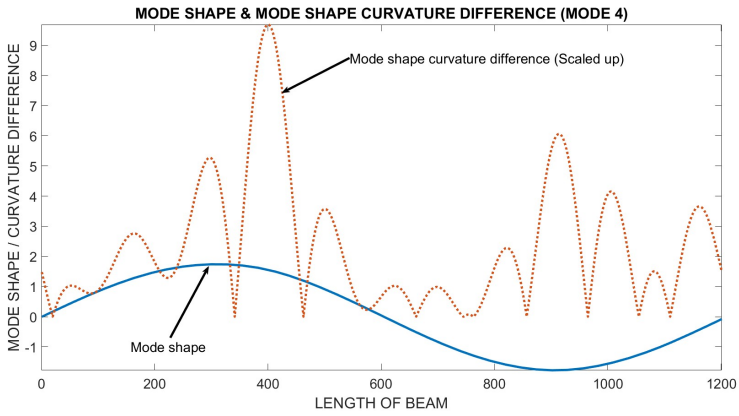

Fig. 7.28: Mode shape - 4 ; curvature difference between 70% damaged (400-410) and 50% damaged (900-910) beams

of the damage as well. However, when it comes to different mode shapes, Figure 7.28 clearly indicates the two defective regions with different intensities while Figure 7.27 indicates only the 70% defective region. This implies that there is an impact from the mode shape as well on the accuracy of the output.

7.9 Mode shape curvature analysis for a portal frame

In previous sections, mode shape curvature analysis was done for a single beam element, but, in this section, the study and the analysis will be continued to a portal frame.

Consider a beam of 150mm x 300mm and two columns of 300mm x 300mm, which makes a portal frame. There, two defective regions were intentionally kept in the beam element, and two other defective regions were in two columns respectively. Figure 7.29 shows the finite element model of the portal frame. Frame elements were used for the finite element analysis. The beam will be denoted as Element 01, Left and Right columns will be denoted as Element 02 and Element 03 respectively. the defective regions are marked in red colour in Figure 7.29.

Element 01 is 6m long having 1201 nodes with 0.005m segments. Element 02 and Element 03 are 4m long each having 801 nodes with 0.005m segments. The defective regions of Element 01 are from nodes 400 to 410 and nodes 900 to 910 out of total nodes of 1201. The defective region of Element 02 is from nodes 200 to 210 out of total nodes of 801. The defective region of Element 03 is from nodes 500 to 510 out of total nodes of 801.

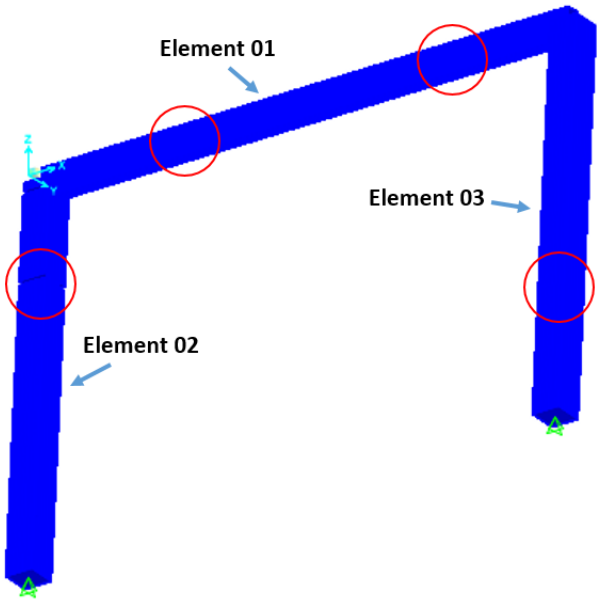

Fig. 7.29: Finite element model of the portal frame showing defective regions in red circles

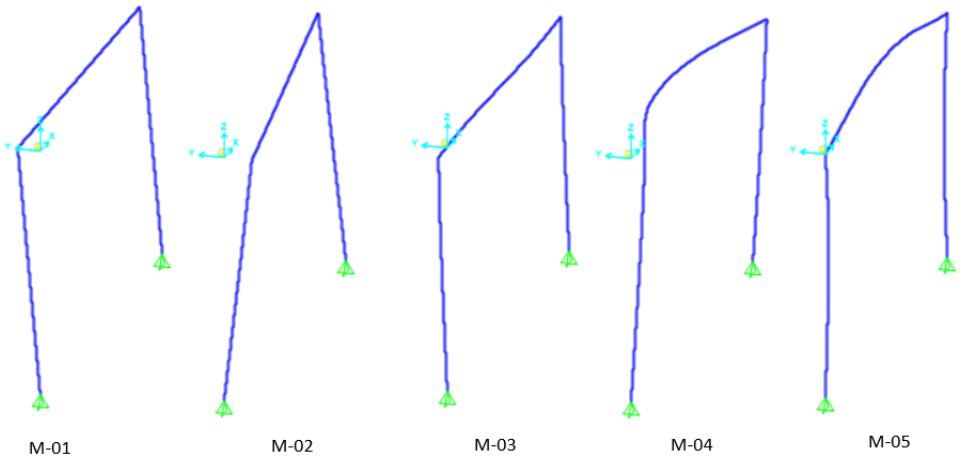

Fig. 7.30: First five mode shapes of the portal frame considered

Figure 7.30 shows different mode shapes of the portal frame. Mode shape 05 was considered for the curvature analysis where the nodal displacements of each element are basically in a 2D plane. Figures 7.31, 7.32, and 7.33 show the mode shape curvature differences along each element and it's clear that the plots are clearly indicating the defective regions of the portal frame. Therefore, this approach is suitable for the detection of defective regions in portal frames as well as showing positive signs for more complex structures.

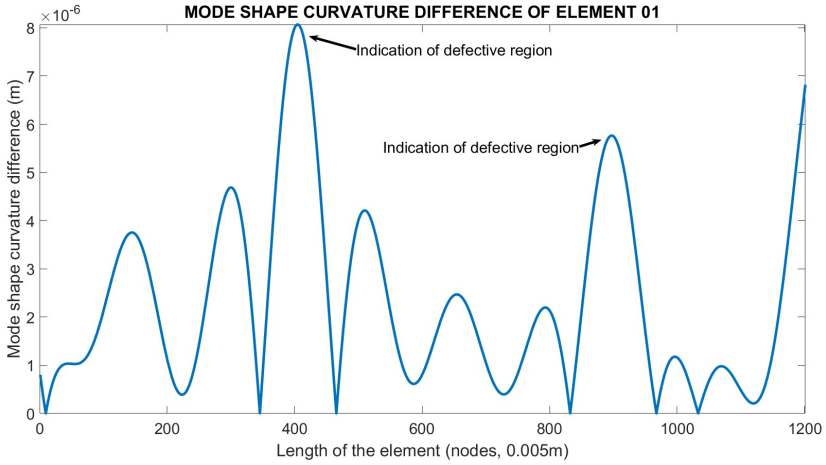

Fig. 7.31: Mode shape curvature difference plot of Element 01 (Mode 5, Defective regions at nodes: 400-410 and 900-910

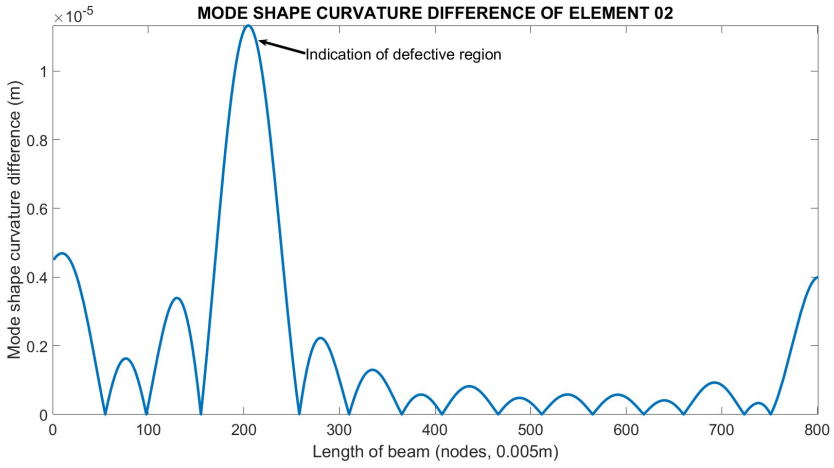

Fig. 7.32: Mode shape curvature difference plot of Element 02 (Mode 5, Defective regions at nodes: 200-210

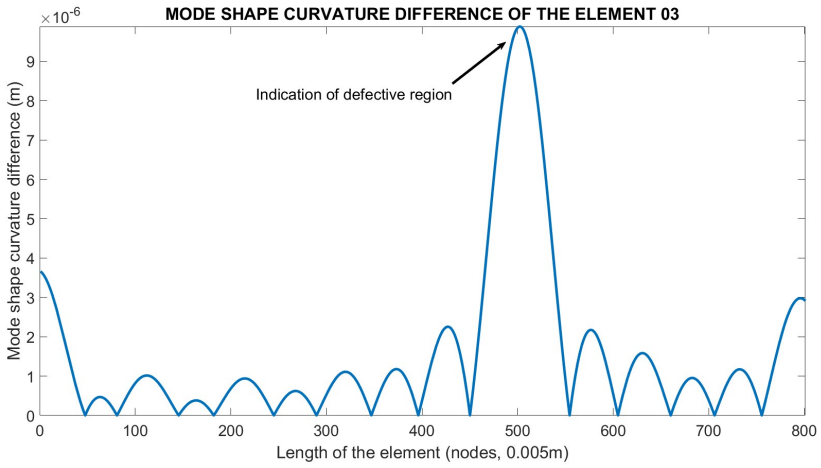

Fig. 7.33: Mode shape curvature difference plot of Element 03 (Mode 5, Defective regions at nodes: 500-510

A drawback encountered here is that the mode shape curvature differences at joints of the structure are also having higher values due to the combined effects of the elements. Therefore, a careful analysis is required in reading the resultant plots. However, defective regions at joints can't be clearly observed with this approach.

7.10 Summary of the mode shape curvature analysis

Mode shape curvature analysis is a successful approach to detecting several defective regions in structural elements. Consider two identical beam elements, except that one beam has certain defective regions where the material properties of those regions are changed compared to the other. This deviation will end up creating deviations in the respective mode shapes of those elements as well. Comparison between mode shapes of those two scenarios is not that much sensitive to identifying the defective regions, but, the respective mode shape curvatures do that as elaborated in previous sections. There are limitations in this approach based on the severity of the defective regions. However, improvements in the finite element model are capable of expanding these limitations. Mode shape is also a significant factor in this regard.

Extracting the mode shape function based on nodal displacement data is the challenging part. The entire process depends on how well a curve is fitted to those nodal displacement data. If that task can be done with a higher level of accuracy, the expected output results are also accurate to a higher level. The second phase of the mode shape curvature analysis is to check whether the approach is applicable to portal frames and found that the mode shape curvature analysis is capable of detecting defects in portal frames as well. This was a significant finding which shows that the approach is showing positive signs in expanding its limitations to more complex structures.

7.11 Practical approaches of the proposed method in real-world structures

This shall be the next stage of this study.

Consider a case where no honeycomb damage can be seen for the naked eye when the element is inspected. However, the contractor or the client wants to ensure that there are no hidden honeycombs as well.

In order to implement the mode shape curvature analysis for this case, first, we have to create an identical finite element model for the selected structural element. From that, the mode shape curvature for the element can be extracted. As the second step, the mode shapes of the actual beam need to be extracted by the use of exciters and mode shape detectable sensors. Then a calibration process for the actual beam and the finite element model has to be followed so as to analyze the mode shape curvature difference for the actual beam and the finite element model. This leads to the identification of the hidden defect. The Figure 7.34 shows the process explained above. This can be started from a structural beam element and later can extend up to an entire structure with appropriate analysis.

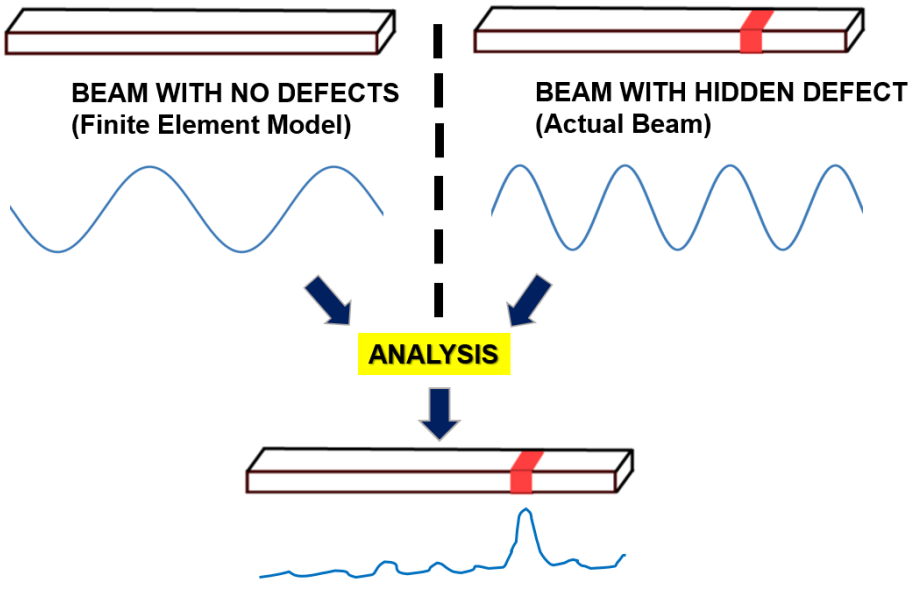

Fig. 7.34: Mode shape curvature analysis process

CHAPTER 8

CONCLUSIONS

This study concludes several significant points related to hidden honeycombs in structural concrete elements as elaborated in this chapter.

8.1 Findings of the study

- A hypothesis was developed explaining the governing factors behind the formation of honeycombs, which is significant in improving remedial actions.
- Based on the field survey and analysis of the findings, a set of guidelines was developed for contractors and designers to mitigate the occurrence of honeycombs.
- A novel mathematical model was developed for mode shape analysis of non-homogeneous structural elements. This mathematical model can be used for development aspects in finite element modelling software.
- This study critically analysed the limitations and positives of mode shape curvature analysis in hidden defect detection, exploring new areas for studies on this. Moreover, the analysis is extended from a single element to portal frames.

8.2 Conclusions

Mode shape curvature analysis for hidden defect detection in structural concrete elements seems a promising approach yet it has its own limitations in implementing with real-world structures and needs more advanced technology and instruments in order to extract the accurate mode shapes of elements. This area is open for further studies and development. Therefore, a combination of conventional non-destructive tests and mode shape curvature analysis will provide a robust approach for hidden defect detection and assessment in structural concrete elements. Well-established detection approaches can be practised for initial investigations and based on that, in-depth analysis and verification for suspicious areas can be done with mode shape curvature analysis for better results.

For the mode shape curvature analysis, the accuracy of the extraction of the mode shape curvature formula based on the nodal displacements in the finite model is significant for analysis. Furthermore, the mathematical approach developed in this study can be utilized for finite element software development for accurate outputs related to mode shape extraction.

The formation of smooth, thin, cement paste layer at the mold face is critical for the visibility of a honeycomb formation from the outside. The hypothesis developed in this study for this phenomenon is important for developing remedial actions for hidden honeycombs.

Most of the defects at the construction stage can be controlled and minimized by the decisions taken at the design stage as well as at the planning stage of a project. Having a better understanding of how the construction activities are carried out is the key to address at these stages. Moreover, understanding of the root cause for each defect observed at site is significant in avoiding the recurrence of the same throughout the project.

Basis for above conclusions are given as a detailed summary below.

8.2.1 Hypothesis on development of smooth, thin cement paste layer on the surface of concrete structures

As per the experiments carried out and the observations, this study provides an explanation on "How the concrete structures have smooth, thin cement paste layer on their surface". During the compaction of fresh concrete, Whenever the cement slurry comes to the surface through air-entrapping paths, it'll create slurry spots on the surface. Further vibration leads to the development of cohesive forces between those slurry spots and creates the smooth, thin cement layer on the surface. Van der Waals forces are weak attractive forces that exist between all molecules. These forces act to bring the cement slurry droplets closer together, allowing them to merge. Capillary action occurs when the cohesive forces within a liquid, such as cement slurry, are stronger than the adhesive forces between the liquid and the mold surface. This causes the liquid to be drawn into narrow spaces, such as the gaps between the droplets, leading to their fusion. Overall, cohesive forces act to bring the individual cement slurry droplets closer together, allowing them to merge and form a continuous surface in the mold. This understanding and explanation is significant in studying the formation of honeycombs.

8.2.2 Root cause analysis in mitigating honeycombs in structural concrete elements

Honeycombs are a commonly found concrete defect in the local construction industry. Honeycombs are first observed by the frontline workers and most of the time they tend to judge the defect and do remedial work not knowing the root cause for the defect. Understanding the root cause for each defect and addressing them is important in avoiding the recurrence of the same defect in future construction. Improving the workmanship of the workers to produce defect-free structures is the biggest challenge

in the field. Proper planning at the design stage of a project and at the initial stage of construction works has the potential to make a huge impact on effortless workmanship improvement of the workers. This has been elaborated under this study and has published a set of guidelines and standard practices for the contractors on mitigating occurrences of honeycombs in concrete structures.

8.2.3 Identification of hidden honeycombs in concrete structures

As elaborated in this study through a set of experiments and analysis, UPV tests have limitations in the identification of hidden honeycombs in concrete structures. Especially, when it comes to heavily reinforced concrete, the test results can be misleading. The results have shown the impact of reinforcement bars going through honeycombs. UPV test fails to identify the surrounding honeycombs as the pulse is transmitted through the reinforcement bars. This shows the significance of moving to other alternative methods for the detection of hidden honeycombs. However, there are limitations in implementing the proposed mode shape curvature analysis in real-world structures due to difficulties in the extraction of accurate mode shapes with available technology. Therefore, a combination of existing damage detection methodology along with modern approaches will provide robust solutions.

8.2.4 Mathematical Modelling and Analysis of Mode Shapes for Non-Homogeneous Structural Elements

This study has developed a novel mathematical approach to analyze the mode shapes of non-homogeneous structural elements. This mathematical model was developed in order to examine the deviations of vibrational patterns between homogeneous and non-homogeneous elements.

Identification of Homogeneous regions and Nonhomogeneous regions in an element and implementing the mathematical model based on the continuity of the element is the key approach presented here. Furthermore, this study has provided an Equation (8.1) that is applicable to any nonhomogeneous single-degree-of-freedom system;

$$P(x) \cdot \Phi''''(x) + 2P'(x) \cdot \Phi'''(x) + P''(x) \cdot \Phi''(x) - \lambda m(x) \cdot \Phi(x) = 0 \qquad (8.1)$$

If the coefficient functions (i.e., Functions of change of properties) can be identified in the above equation, the equation can produce the mode shape of that non-homogeneous element. However, the identification of coefficient functions is not that simple. Therefore, this study has carried out another novel approach for the sample calculation. The sample calculation in this study has been provided for a beam element having reduced stiffness in a certain region, which is similar to a defective region of a

structural element. Identification of Homogeneous regions and Non-homogeneous regions in an element and implementing the mathematical model based on the continuity of the element is the key approach presented here and it has been successful.

8.2.5 Mode shape curvature analysis

The other approach of this study is the mode shape curvature analysis between homogeneous and non-homogeneous elements. Mode shape curvature analysis is a successful approach to detecting several defective regions in structural elements. Consider two identical beam elements except one beam has certain defective regions where the material properties of those regions are changed compared to the other. This deviation will end up creating deviations in the respective mode shapes of those elements as well. Comparison between mode shapes of those two scenarios is not that much sensitive in identifying the defective regions, but, the respective mode shape curvatures do that as elaborated in previous sections. There are limitations in this approach based on the severity of the defective regions. However, improvements in the finite element model are capable of expanding these limitations. Mode shape is also a significant factor in this regard. Extracting the mode shape function based on nodal displacement data is the challenging part. The entire process depends on how well a curve is fitted to those nodal displacement data. If that task can be done with a higher level of accuracy, the expected output results are also accurate to a higher level. However, there are practical difficulties and limitations in implementing the said approach for real-world structures which needs more research and development.

The second phase of the mode shape curvature analysis is to check whether the approach is applicable to portal frames and found that the mode shape curvature analysis is capable of detecting defects in portal frames as well. This was a significant finding that shows that the approach is showing positive signs in expanding its limitations to more complex structures.

8.3 Recommendations for future works

An experimental approach to detect hidden honeycombs by using mode shape curvature analysis shall be the next step of this study. Accuracy in extracting mode shapes of the concrete elements is important in this regard. A lot more research and developments are required to extract mode shapes of concrete elements in real-world structures. Furthermore, this approach can be developed in a way such that an entire structure can be examined for any hidden defects or honeycombs.

The use of Artificial Intelligence (AI) techniques to detect hidden honeycombs in concrete structures shall be another step in developing this approach. The mode shape

curvature pattern analysis of various cases and development shall be one path in this regard. The behavioural patterns of the mode shapes in non-homogeneous elements can be utilized for this.[38]

REFERENCES

[1] Federal Highway Administration (FHWA), "Concrete pavement preservation guide - chapter 6: Full-depth repair," Website, n.d. [Online]. Available: https://www.fhwa.dot.gov/publications/research/infrastructure/pavements/pccp/04150/chapt6.cfm

[2] A. N. Talbot, *Concrete Construction and Concrete Failures*. New York: Engineering News Publishing Company, 1905.

[3] T. Potter, *Concrete: Its Nature and Uses*. London: Crosby Lockwood and Son, 1910.

[4] W. H. Hebard, "A study of honeycombs in concrete," *Proceedings of the American Concrete Institute*, vol. 20, pp. 103–123, 1924.

[5] A. Pandey, M. Biswas, and M. Samman, "Damage detection from changes in curvature mode shapes," *Journal of Sound and Vibration*, vol. 145, no. 2, pp. 321–332, 1991.

[6] J. Smeaton, "A narrative of the building and a description of the construction of the Eddystone lighthouse with stone," *Philosophical Transactions of the Royal Society*, vol. 51, no. 2, pp. 61–82, 1759.

[7] J. Aspdin, "Improvements in the manufacture of Portland cement," *London Journal of Arts and Sciences*, vol. 6, pp. 368–372, 1824.

[8] K. Walz, *Vibrated Concrete (Ruttelbeton)*, 3rd ed. Berlin: Wilhelm Ernst and Son, 1960.

[9] J. Kolek, "Research on the vibration of fresh concrete," in *Reports, Conference on Vibrations–Compaction Techniques, Julius Hoban*, Budapest, 1963.

[10] R. L'Hermite and G. Tournon, "Vibration of fresh concrete (la vibration du béton frais)," *Annles, Institut Technique du Batiment et des Travaux Publics (Paris)*, 1948.

[11] R. H. H. Kirkham, "The compaction of concrete by surface vibration," *Reports, Conference on Vibration-Compaction Techniques*, pp. 251–268, 1963.

[12] R. W. Taylor, *The Compaction of Concrete by Internal Vibrators—An Investigation of the Effects of Frequency and Amplitude*. London: Cement and Concrete Association, 1976, publication No. 42.511.

[13] A. M. Alexander, "Study of vibration in concrete; mechanics of motion of fresh concrete," U.S. Army Engineer Waterways Experiment Station, Vicksburg, MS, Tech. Rep. Technical Report No. 6-780, Report 3, Sept. 1977.

[14] K. Iida and S. Horigome, "Properties of double-mixed lean concrete subjected to vibrating compaction," in *Consolidation of Concrete*, ser. SP-96, S. H. Gebler, Ed. Farmington Hills, MI: American Concrete Institute, 1987, pp. 215–246.

[15] L. L. Galappaththi, K. K. A. Perera, and A. K. Jayawardana, "Investigation on structural issues caused due to lack of quality assurance and quality control (qa/qc) practices and methods to rectify the observed issues in construction sites," in *Annual sessions, Institute of Engineers, Sri Lanka*, 2016, pp. 28–34.

[16] R. Savitha, "Importance of quality assurance of materials for construction work," Building Materials Research and Testing Division, National Building Research Organization, 2012. [Online]. Available: https://nbro.gov.lk/images/content_image/publications/symposia/2010/importance_of_quality_assurance.pdf

[17] N. Jamaluddin, S. S. Ayop, M. H. Wan Ibrahim, K. H. Boon, D. Yeoh, S. Shahidan, N. Mohamad, T. N. Tuan Chik, N. H. Abd. Ghafar, A. H. Abdul Ghani, and S. Shamrul-Mar, "Forensic building: Deterioration and defect in concrete structures," in *MATEC Web of Conferences*, vol. 1030, no. 2. EDP Sciences, November 2017, p. 02016.

[18] ASTM C31/C31M-21, "Standard practice for making and curing concrete test specimens in the field," Standard, ASTM International, 2021. [Online]. Available: https://www.astm.org/Standards/C31.htm

[19] A. M. Neville, *Properties of Concrete*. Pearson Education Limited, 2011.

[20] P. K. Mehta and P. J. M. Monteiro, *Concrete: Microstructure, Properties, and Materials*. McGraw-Hill Education, 2013.

[21] C. Sikorsky, "Development of a health monitoring system for civil structures using a level-4 non-destructive damage evaluation method," in *Proc., the 2nd International Workshop on Structural Health Monitoring*, 1999, pp. 68–81.

[22] A. Rytter, "Vibration based inspection of civil engineering structures," Ph.D. dissertation, Department of Building Technology and Structural Engineering, Aalborg University, 1993.

[23] M. Karbhari and L. S.-W. Lee, "Vibration-based damage detection techniques for structural health monitoring of civil infrastructure systems," in *Woodhead Publishing Series in Civil and Structural Engineering*, 2009, pp. 177–212.

[24] C. Farrar and H. Sohn, "Condition/damage monitoring methodologies," in *The Consortium of Organizations for Strong Motion Observation Systems (COSMOS) Workshop*, Emeryville, CA, November 2001, pp. 14–15, invited Talk.

[25] M. Green, "Modal test methods for bridges: A review," in *Proceedings of the 13th International Modal Analysis Conference*, Nashville, Tennessee, 1995, pp. 552–558.

[26] H. Adeli and S. Hung, *Machine Learning – Neural Networks, Genetic Algorithms, and Fuzzy Systems*. John Wiley & Sons, 1995.

[27] S. Hassiotis, "Identification of damage using natural frequencies and Markov Parameters," *Computers and Structures*, pp. 365–373, 2000.

[28] S. Doebling, C. Farrar, M. Prime, and D. Shevitz, "Damage identification and health monitoring of structural and mechanical systems from changes in their vibration characteristics: A literature review," Los Alamos National Laboratory, Tech. Rep. LA-13070-MS, May 1996.

[29] S. Law, Z. Shi, and L. Zhang, "Structural damage detection from incomplete and noisy modal test data," *Journal of Engineering Mechanics*, pp. 1280–1288, 1998.

[30] V. Dawri and G. Vesmawla, "Modal curvature and modal flexibility methods for honeycomb damage," *Procedia Engineering*, vol. 51, pp. 119–124, 2013.

[31] Z. Ismail, D. Samugavelu, and H. Abdul Razak, "Algorithm for detecting honeycombs in rc beams," *Asian Journal of Civil Engineering (Building and Housing)*, vol. 8, no. 5, p. 563, 2007.

[32] H. R. Kumavat, N. R. Chandak, and I. T. Patil, "Factors influencing the performance of rebound hammer used for non-destructive testing of concrete members: A review," *Case Studies in Construction Materials*, vol. 15, p. e00491, 2021.

[33] T. K. Makarios, "Identification of eigen-frequencies and mode-shapes of beams with continuous distribution of mass and elasticity and for various conditions at supports," *Number Theory and Its Applications*, vol. IntechOpen, May 2020.

[34] R. Vaicaitis, "Free vibrations of beams with random characteristics," Department of Civil Engineering and Engineering Mechanics, Columbia University, New York, New York 10027, U.S.A., Technical Report, 1974.

[35] S. Abrate, "Vibration of non-uniform rods and beams," Department of Technology, Southern Illinois University at Carbondale, Carbondale, Illinois 62901-6603, U.S.A., Technical Report, 1994.

[36] F. Sohani and H. Eipakchi, "Analytical Solution for Modal Analysis of Euler-Bernoulli and Timoshenko Beam with an Arbitrary Varying Cross-Section," Faculty of Mechanical and Mechatronics Engineering, Shahrood University of Technology, 2018.

[37] S. Abdelghany, K. Ewis, A. Mahmoud, and M. Mohamed, "The vibration of a circular beam with variable cross sections using differential transformation method," vol. 361, pp. 164–177, Sep. 2015.

[38] K. A. B. P. Kuruppu and K. Baskaran, "Mathematical modelling and analysis of mode shapes for non-homogeneous structural elements: Based on first principles," in *Annual Sessions of Society of Structural Engineers, Sri Lanka.*, 2023.

APPENDIX A

MATLAB CODES

The MATLAB code used for mode shape curvature analysis is given in Appendix A

```
syms x
%% M4 normal beam
fn=(170909083842919*sin((52*x)/625 - 1267/1000))/4611686018427387904 + (8779*sin((21*x)/2000
+ 3901/1250))/5000 + (4462857687240699*sin((603*x)/10000 - 141/250))/73786976294838206464 +
(5059499177560761*sin((63*x)/1250 - 6837/10000))/73786976294838206464 +
(2020102943511933*sin((309*x)/10000 - 4199/5000))/18446744073709551616 +
(3684478874306451*sin((383*x)/10000 - 641/10000))/36893488147419103232 +
(3146276669211901*sin((711*x)/10000 - 7361/10000))/73786976294838206464 +
(4781838785763285*sin((33*x)/1250 - 19683/10000))/73786976294838206464
fnD=((8779*sin((13*x)/2500 - 13/2500))/5000)
fn4=(8779*sin((13*x)/5000 - 13/5000))/5000
fnM2=(8779*sin((13*x)/5000 - 13/5000))/5000

%%M4 - 200-205 and 450-455 E10%
f1=((621*sin((49*x)/2500 + 397/5000))/5000 + (13*sin((31*x)/500 - 6873/5000))/1000 +
(49*sin((311*x)/10000 - 1373/2500))/1250 + (6611*sin((89*x)/10000 + 4477/1250))/2500 +
(11*sin((409*x)/10000 + 4349/2000))/625 + (19*sin((569*x)/5000 + 4861/10000))/5000 +
(11891*sin((53*x)/10000 + 7603/5000))/10000 + (7*sin((877*x)/10000 - 4203/10000))/1000)


%%M4 - 200-205 and 450-455 E20%
f2=-((13*sin((31*x)/500 + 3531/2000))/2000 + (1371*sin((6*x)/625 + 1109/5000))/625 +
(23*sin((61*x)/2000 + 3511/1250))/1250 + (101*sin((403*x)/10000 - 299/400))/10000 +
(7*sin((219*x)/2500 - 8801/2500))/2000 + (2737*sin((31*x)/5000 + 21871/5000))/5000 +
(27*sin((193*x)/10000 + 32009/10000))/400 + (19*sin((1139*x)/10000 + 36137/10000))/10000)


%%M4 - 200-205 and 450-455 E30%
f3=(11*sin((72*x)/625 - 187/1250))/10000 + (51*sin((11*x)/2000 - 454/625))/5000 +
sin((839*x)/10000 + 853/1250)/625 + (187*sin((207*x)/10000 - 7747/10000))/10000 +
(37*sin((157*x)/2500 - 15957/10000))/10000 + (27*sin((317*x)/10000 - 9223/10000))/2500 +
(51*sin((419*x)/10000 + 19641/10000))/10000 + (8753*sin((21*x)/2000 + 31073/10000))/5000


%%M4 - 200-205 and 450-455 E40%
f4=-((2191*sin((21*x)/2000 - 73/2500))/1250 + sin((13*x)/625 + 5849/2500)/80 +
(63*sin((13*x)/2500 + 5069/2000))/10000 + sin((419*x)/5000 - 4947/2000)/1000 +
(33*sin((419*x)/10000 - 2959/2500))/10000 + (73*sin((63*x)/2000 + 11299/5000))/10000 +
(207450930931433*sin((72*x)/625 + 14773/5000))/288230376151711744 + (3*sin((157*x)/2500 +
15561/10000))/1250)


%%M4 - 200-205 and 450-455 E50%
f5=-((17541*sin((21*x)/2000 - 263/10000))/10000 + (11*sin((419*x)/10000 - 2391/2000))/5000 +
(17*sin((157*x)/2500 + 7867/5000))/10000 + (51*sin((157*x)/5000 + 23003/10000))/10000 +
(4644613456598959*sin((72*x)/625 + 29149/10000))/9223372036854775808 +
(1595089960053665*sin((419*x)/5000 - 25123/10000))/2305843009213693952 +
(43*sin((209*x)/10000 + 23071/10000))/5000 + (21*sin((53*x)/10000 + 26121/10000))/5000)
f5D=(351*sin((13*x)/2500 - 27/2500))/200 + (3*sin((419*x)/10000 - 2283/1000))/5000 +
(37*sin((13*x)/5000 + 7237/2500))/10000 + (23*sin((209*x)/10000 - 5477/5000))/10000 +
(23*sin((159*x)/10000 + 10921/5000))/5000 + sin((471*x)/10000 + 7711/10000)/2000 +
sin((157*x)/5000 + 15121/10000)/625 + (41*sin((103*x)/10000 + 23669/10000))/5000
```

```
%%M4 - 200-205 and 450-455 E60%
f6=-((3*sin((209*x)/5000 - 2977/2500))/2000 + (19*sin((59*x)/10000 + 433/200))/5000 +
(1096*sin((21*x)/2000 - 253/10000))/625 + (11*sin((157*x)/2500 + 7973/5000))/10000 +
(411696740080059*sin((72*x)/625 + 14349/5000))/1152921504606846976 + (17*sin((157*x)/5000 +
23113/10000))/5000 + (8674027998339705*sin((419*x)/5000 - 25769/10000))/18446744073709551616
+ (29*sin((209*x)/10000 + 23139/10000))/5000)


%%M4 - 200-205 and 450-455 E70%
f7=-((877*sin((21*x)/2000 - 119/5000))/500 + (2324843155609615*sin((72*x)/625 +
6993/2500))/9223372036854775808 + (4249161380518811*sin((209*x)/5000 -
3063/2500))/4611686018427387904 + (7080782712693411*sin((157*x)/2500 +
8163/5000))/9223372036854775808 + (7*sin((59*x)/10000 + 10189/5000))/2500 +
(23*sin((157*x)/5000 + 23259/10000))/10000 + (2875478466209845*sin((419*x)/5000 -
26757/10000))/9223372036854775808 + (19*sin((209*x)/10000 + 23289/10000))/5000)


%%M4 - 200-205 and 450-455 E80%
f8=-((803032886388761*sin((72*x)/625 + 1343/500))/4611686018427387904 +
(453789904213255*sin((419*x)/5000 - 2857/1000))/2305843009213693952 + (877*sin((21*x)/2000 -
229/10000))/500 + (23*sin((209*x)/10000 + 1474/625))/10000 +
(8860155646043435*sin((629*x)/10000 + 1701/1000))/18446744073709551616 +
(4638157096173161*sin((417*x)/10000 - 3231/2500))/9223372036854775808 + (23*sin((4*x)/625 +
17259/10000))/10000 + (7*sin((157*x)/5000 + 23543/10000))/5000)


%%M4 - 200-205 and 450-455 E90%
f9=-((1074799543454687*sin((72*x)/625 + 997/400))/9223372036854775808 +
(17549*sin((21*x)/2000 - 27/1250))/10000 + (4806114700964287*sin((157*x)/2500 +
2337/1250))/18446744073709551616 + (8796883313870611*sin((419*x)/5000 +
6089/2000))/73786976294838206464 + (6741639322898261*sin((157*x)/5000 +
6033/2500))/9223372036854775808 + (3*sin((209*x)/10000 + 3037/1250))/2500 +
(6645992954876077*sin((209*x)/5000 - 8457/5000))/36893488147419103232 + (3*sin((57*x)/10000 +
17807/10000))/2500)
f9D=sin((157*x)/10000 + 567/250)/2000 + sin((157*x)/5000 + 3781/2500)/5000 +
(8779*sin((13*x)/2500 - 59/10000))/5000 + sin((471*x)/10000 + 3771/5000)/10000 +
(3*sin((209*x)/10000 - 10907/10000))/10000 + (9*sin((21*x)/2000 + 22783/10000))/10000 +
sin((419*x)/10000 - 22823/10000)/10000 + sin((13*x)/5000 + 30193/10000)/2500
f94=sin((59*x)/2500 + 3671/5000)/10000 + sin((79*x)/10000 + 1413/625)/2000 + sin((13*x)/10000
+ 1893/625)/2500 + (8779*sin((13*x)/5000 - 33/10000))/5000 + sin((209*x)/10000 -
5761/2500)/10000 + (9*sin((13*x)/2500 + 11349/5000))/10000 + (3*sin((21*x)/2000 -
11021/10000))/10000 + sin((157*x)/10000 + 14993/10000)/5000


f95D=-(sin((21*x)/2000 - 1727/2000)/2500 + sin((13*x)/5000 - 153/1250)/5000 +
(3*sin((157*x)/10000 - 546/625))/10000 + sin((157*x)/5000 - 16291/10000)/10000 +
sin((209*x)/10000 + 20509/10000)/10000 + (8779*sin((13*x)/2500 + 31361/10000))/5000)



f95=-(sin((13*x)/2500 - 1969/2500)/2000 + sin((21*x)/2000 + 4129/2000)/10000 +
sin((157*x)/10000 - 4107/2500)/10000 + sin((13*x)/10000 - 2377/10000)/5000 +
(3*sin((79*x)/10000 - 9497/10000))/10000 + (8779*sin((13*x)/5000 + 31387/10000))/5000)
```

```
fm=-((63*sin((51*x)/5000 - 7153/5000))/1000 + (3*sin((183*x)/5000 - 3357/10000))/625 +
(243*sin((157*x)/10000 - 1287/10000))/10000 + (131*sin((211*x)/10000 + 6951/5000))/10000 +
(3529*sin((13*x)/2500 + 15553/5000))/2000 + (18*sin((3*x)/1250 - 18169/5000))/625 +
(4*sin((321*x)/10000 - 20269/10000))/625 + (41*sin((13*x)/500 - 32159/10000))/5000)


fm2=(3*sin((13*x)/500 - 47/1000))/400 + sin(x/400 - 1449/5000)/50 + (71*sin((159*x)/5000 +
1293/1000))/10000 + (1099*sin((13*x)/2500 - 369/10000))/625 + (131*sin((21*x)/1000 -
8073/5000))/10000 + (609*sin((103*x)/10000 + 8667/5000))/10000 + (49*sin((79*x)/5000 +
28697/10000))/2000 + (43*sin((183*x)/5000 + 28701/10000))/10000
%% 50% and 90%


fm3=(33*sin((13*x)/1250 + 229/80))/2500 + (8773*sin((13*x)/2500 - 7/625))/5000 +
(39*sin((209*x)/10000 - 519/625))/10000 + (41*sin((157*x)/10000 + 4931/2500))/5000 +
(117*sin((13*x)/5000 + 15239/5000))/10000 + sin((157*x)/5000 + 15547/10000)/400 +
(3*sin((131*x)/5000 - 25019/10000))/2500 + (11*sin((419*x)/10000 - 25189/10000))/10000
%% 30% and 50%


fm4=-((17559*sin((13*x)/5000 - 3/1000))/10000 + (7177074716758175*sin((21*x)/1000 -
921/5000))/9223372036854775808 + (83*sin((51*x)/10000 + 281/2500))/10000 +
(7077646766200881*sin((367*x)/10000 - 2349/5000))/18446744073709551616 +
(19*sin((157*x)/10000 + 5887/5000))/10000 + (6502200584821511*sin((131*x)/5000 -
14601/5000))/9223372036854775808 + (1379908690433843*sin((157*x)/5000 +
12753/10000))/4611686018427387904 + (39*sin((21*x)/2000 - 25197/10000))/10000)
%% Mode 2 - 30% and 50%


Kn = ((diff(diff(fn)))/((1+((diff(fn))^2))^1.5))
KnD=((diff(diff(fnD)))/((1+((diff(fnD))^2))^1.5))
Kn4=((diff(diff(fn4)))/((1+((diff(fn4))^2))^1.5))


KnM2=((diff(diff(fnM2)))/((1+((diff(fnM2))^2))^1.5))


K1 = ((diff(diff(f1)))/((1+((diff(f1))^2))^1.5))
K2 = ((diff(diff(f2)))/((1+((diff(f2))^2))^1.5))
K3 = ((diff(diff(f3)))/((1+((diff(f3))^2))^1.5))
K4 = ((diff(diff(f4)))/((1+((diff(f4))^2))^1.5))


K5 = ((diff(diff(f5)))/((1+((diff(f5))^2))^1.5))
K5D = ((diff(diff(f5D)))/((1+((diff(f5D))^2))^1.5))


K6 = ((diff(diff(f6)))/((1+((diff(f6))^2))^1.5))
K7 = ((diff(diff(f7)))/((1+((diff(f7))^2))^1.5))
K8 = ((diff(diff(f8)))/((1+((diff(f8))^2))^1.5))


K9 = ((diff(diff(f9)))/((1+((diff(f9))^2))^1.5))
```

```
K9D = ((diff(diff(f9D)))/((1+((diff(f9D))^2))^1.5))
K94 = ((diff(diff(f94)))/((1+((diff(f94))^2))^1.5))


K95D = ((diff(diff(f95D)))/((1+((diff(f95D))^2))^1.5))


K95 = ((diff(diff(f95)))/((1+((diff(f95))^2))^1.5))


Km = ((diff(diff(fm)))/((1+((diff(fm))^2))^1.5))
%% 10% and 90%


Km2=((diff(diff(fm2)))/((1+((diff(fm2))^2))^1.5))


Km3=((diff(diff(fm3)))/((1+((diff(fm3))^2))^1.5))
%% 30% and 50%


Km4=((diff(diff(fm4)))/((1+((diff(fm4))^2))^1.5))
%% Mode 2 - 30% and 50%


deltaK1= abs(K1-Kn)
deltaK2= abs(K2-Kn)
deltaK3= abs(K3-Kn)
deltaK4= abs(K4-Kn)


deltaK5= abs(K5-Kn)
deltaK5D= abs(K5D-KnD)


deltaK6= abs(K6-Kn)
deltaK7= abs(K7-Kn)
deltaK8= abs(K8-Kn)


deltaK9= abs(K9-Kn)
deltaK9D= abs(K9D-KnD)
deltaK94= abs(K94-Kn4)


deltaK95D= abs(K95D-KnD)


deltaK95= abs(K95-Kn4)


deltaKm=abs(Km-KnD)
%%10% and 90%
```

```
deltaKm2=abs(Km2-KnD)
%%50% and 90%


deltaKm3=1000000*abs(Km3-KnD)
%%30% and 50% well working - Mode 4


deltaKm4=1000000*abs(Km4-KnM2)
%%30% and 50% well working - Mode 2


deltaf1= abs(f1-fn)
deltaf2= abs(f2-fn)
deltaf3= abs(f3-fn)
deltaf4= abs(f4-fn)
deltaf5= abs(f5-fn)
deltaf6= abs(f6-fn)
deltaf7= abs(f7-fn)
deltaf8= abs(f8-fn)
deltaf9= abs(f9-fn)


fplot([deltaK1 deltaK3 deltaK5 deltaK7 deltaK9],[1,601])
```